NONTHEMAL PLASMA SYNTHESIS OF INDIUM PHOSPHIDE NANOCRYSTALS AND ELECTRICAL PROPERTIES OF DOPED SILICON NANOCRYSTAL FILMS

A THESIS
SUBMITTED TO THE FACULTY OF THE GRADUATE SCHOOL
OF THE UNIVERSITY OF MINNESOTA
BY

Ryan Gerard Gresback

IN PARTIAL FULFILLMENT OF THE REQUIREMENTS
FOR THE DEGREE OF
MASTER OF SCIENCE

Professor Uwe Kortshagen

February 2010

Acknowledgements

I would like to first thank my adviser, Professor Uwe Kortshagen, for providing me the unique opportunity to work with him for so many years. He was kind and courageous enough to allow me as a high school student to start working in his lab. Little did he realize at the time, I would not leave until almost seven years later. I am extremely grateful for all the guidance, opportunities, and wide range of research topics Professor Kortshagen has given me.

I want to thank many of my colleagues throughout the years for their help and support. I would like to specifically thank Mike Hebert for introducing me to the lab. I would also like to thank my officemates Chin-Yi Liu and Zak Holman. My lab-mates, Italian friends, and Sally's cohorts Lorenzo Mangolini, Federico Galli, and Patrizio Cernetti for providing a great deal of support for both the mind and the soul. I would also like to thank the entire HTPL group as the lab has been a second home for me, and every day it felt like one.

I would like to thank my parents and brother for providing me with constant support and encouragement. Without their support and encouragement this thesis would not have been possible. I would like to thank Naoko for supporting me and reminding me that there is sometimes a world beyond the lab.

Abstract

This thesis is concerning the plasma synthesis of semiconductor nanocrystals (NCs). Two systems of nanocrystals were studied, indium phosphide and doped silicon. A new method of synthesis of InP NCs is presented. It represents a new route for the synthesis of high quality compound semiconductor NCs. Additionally the electronic properties of doped silicon NCs were studied as a function of the doping concentration.

Indium phosphide nanocrystals (InP NCs) were synthesized using a nonthermal plasma. The NCs were synthesized using a simple capacitively coupled plasma where the precursors are flowed through a 3/8" quartz tube with two outer ring electrodes. The size of the NCs was primarily controlled through the residence time of the NCs in the plasma. Residence times of 2-10 ms lead to particles with mean sizes between ~2.5-4 nm with size distributions less than 25% of the mean particle size. The mass yield for this system was found to be up to 40 mg/hr. When a ZnS shell was grown around the InP NCs, size-tunable emission from the blue-green to the red was observed. Quantum yields as high as 15% were observed with this synthesis route. This route allows for synthesis of free-standing NCs that can be easily manipulated with colloidal based techniques or included in devices without stabilizing ligands.

The electrical conductivity of phosphorus doped Si NCs was studied as a function of the doping concentration. Doped Si NCs with mean sizes of 8-13 nm were spun cast onto a

substrate with pre-deposited aluminum electrodes. The spin cast process produces films with zero to several monolayers of NCs. The conductivity of the films varies continuously from 10^{-11} S/cm for intrinsic NCs to 10^{-1} S/cm for highly doped NCs. These results indicate that the dopants are electrically active. The interpretation of these results means that the electronic properties of NCs can be tuned in a similar fashion as bulk semiconductors by introducing dopants. The ability to successfully dope NCs can have broad impact on the ability to form semiconductor devices.

Table of Contents

List of Figures

Chapter 1

1.1 Chapter Overview

This chapter introduces the topic of nanocrystal synthesis. First nanocrystals are introduced generally and important previous work is discussed. A discussion of the synthesis of InP nanocrystals using liquid phase techniques follows. Nonthermal plasma synthesis of nanocrystals is introduced to give the reader a background on the current methods and materials. Finally, this chapter discusses the interest in and background of doped Si nanocrystals.

1.2 Nanocrystals

Crystalline semiconductor materials with diameters less than 100 nm are referred to as nanocrystals (NCs). When the diameter of NCs is less than twice the Bohr radius, the NC optical and electronic properties deviate from bulk properties. NCs which exhibit properties that deviate from the bulk are referred to as quantum dots (QD).[1] An implication of size-tunable properties is that one material can exhibit a wide range of properties. The ability to control bandgap, absorption, and emission[2] are ideal for applications such as QD sensitized solar cells,[3] biological tagging,[4] QD LEDs[5], QD solar cells,[3] and hybrid organic-NC devices.[6]

Early work on the development and characterization of NCs was focused on II-VI materials.[7, 8] A robust method to synthesize II-VI NCs that exhibit size-tunable optical

properties was developed in the mid '90s.[9] Figure 1.1 shows the bandgap of CdSe as a function of size. These near monodisperse samples exhibit narrow photoluminescence (PL) peaks and discrete absorption features, as is highlighted in Figure 1.2. While synthesis of high quality II-VI NCs is well developed, concerns about the toxicity and scarcity of the constituent materials remain. This concern has led to the study of other semiconductor materials that are more abundant and less toxic. Some materials of interest include III-V and Group IV materials.

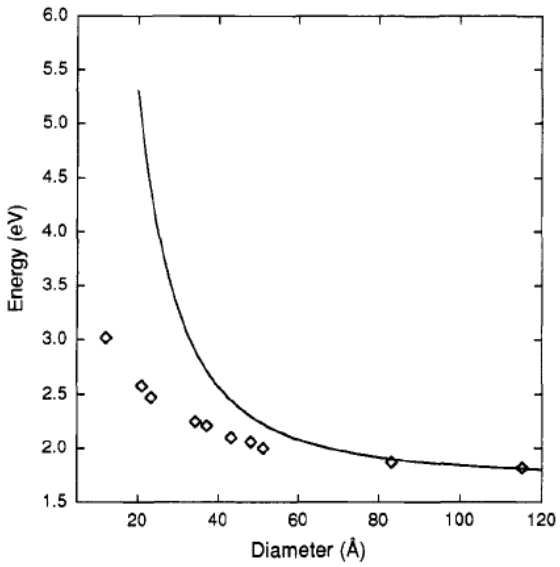

Figure 1.1: Bandgap shift of CdSe NCs as a function of NC size. Diamonds represent experimental work and solid line is predicted by effective mass approximation. Reproduced from reference 9.

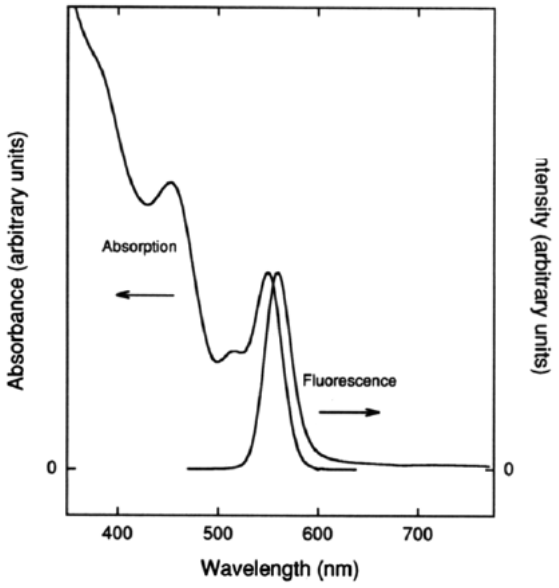

Figure 1.2: Absorption and Flourescene of CdSe NCs. Reproduced from reference 9.

1.3 Indium Phosphide Nanocrystals

InP NCs have received significant attention as they are less toxic than II-VI materials and exhibit optical properties which may be tuned from the near-infrared through the visible spectrum. Liquid-phase synthesis of InP NCs was developed during the same period that II-VI synthesis methods were discovered; however, reaction times were up to 7 days and optical properties were not as good as for II-VI NCs.[10, 11] These long reaction times were a concern as it was not an economically viable way to synthesize NCs. Much of the early work on InP NCs was done using similar chemistry as was used for II-VI materials. Trioctylphosphine oxide (TOPO) and trioctylphosphine (TOP) showed great results for CdSe nanocrystals as the stabilizing agent in colloidal reactions; therefore, it was believed that they would work similarly for InP NCs.

However, it was later discovered that long reaction times were overcome by using different coordinating solvents and precursors. Fatty acids such as myristic acid reduced reaction times and resulted in more uniformly sized of NCs.[12] The new methods required 3-4 hours per batch. However photoluminescence quantum yields were still low, at values less than a couple of percent. It was discovered that P dangling bonds at the surface of InP NCs were the cause of low quantum yields.[13] Methods were proposed to either remove the phosphorus dangling bonds at the surface by HF acid etching,[13, 14] or by using a wide-bandgap semiconductor, such as ZnS, to epitaxially grown a shell around the InP NC core in solution.[15, 16, 17] These methods have allowed for InP NCs that exhibit high quantum yields of 30-60% at room temperature.

Figure 1.3 shows example PL and absorption spectra for InP nanocrystals which have had a ZnS shell grown around them.[15] The PL peak intensity of these NCs changes from blue to the near infrared with increasing. Correspondingly, the onset of absorption changes from the blue to the near infrared. While wet chemical techniques are now able to produce high quality InP NCs, additional synthesis routes which may be run continuously and produce free-standing material are of interest. In Chapter 2, a method to produce InP NCs via a nonthermal plasma is introduced.

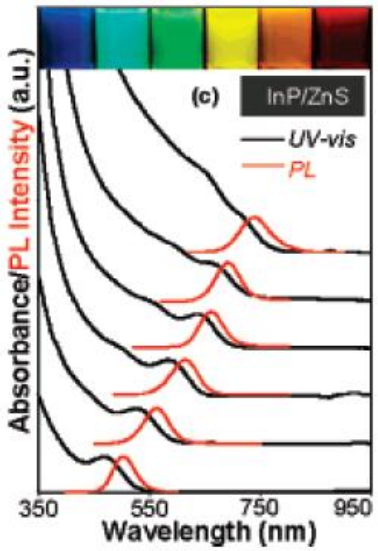

Figure 1.3: PL and absorption spectra of InP/ZnS core/shell structures. Reproduced from reference 15.

1.4 Nonthermal Plasma Synthesis of Nanoparticles

Gas phase approaches to nanoparticle synthesis have been studied extensively. Methods include flame spray pyrolysis,[18] thermal (hot wall) reactors,[19] laser pyrolysis,[20] and ultrasonic aerosol pyrolysis.[21] Generally, these methods require high temperatures to dissociate precursors and nucleate crystalline material. Each method has limitations. Flame spray pyrolysis requires oxidizers to be a main component in the precursor, lending itself to oxide nanoparticle synthesis. Flame spray pyrolysis is often used in manufacturing of TiO_2 nanoparticles for pigments and cosmetics.[18] Thermal reactors tend to yield material which is coalesced and has a wide size distribution. Laser pyrolysis requires high powered lasers to dissociate the precursors thermally. Gas phase systems provide high throughputs; however, due to their thermal nature the materials produced

are often coalesced and agglomerated.[22] Alternatively, nonthermal plasmas offer a synthesis route which can provide freestanding material.

Due to the unique environment of nonthermal plasmas, precursors can be dissociated at low temperatures through high energy electrons. Additionally, aggregation of NCs is suppressed due to Coulomb forces caused by unipolar charging. The NCs are negatively charged due to the characteristically high electron temperatures (1-10 eV), while the gas and ion temperatures remain near ambeint.[23] The other phenomenon which is characteristic of plasmas is heating of NCs due to electron-ion recombination at NC surfaces.[24]

Much of the early work on NCs in nonthermal plasmas was done with silane (SiH_4)-containing discharges; this is due to the semiconductor industry's interest in using plasma-enhanced chemical vapor deposition (PECVD) for various Si layers in devices.[25] The nucleation and growth of Si NCs was studied extensively in the 1990s.[26, 27]
It was discovered in the early 1990s that nano-sized Si showed unique optical properties.[28] This led to the use of nonthermal plasmas specifically designed to synthesize Si NCs. A very high frequency plasma (VHF) reactor developed by Oda's group showed promising results for the synthesis of freestanding Si NCs.[29, 30] Other reactor designs have been proposed since, including inductively coupled (ICP),[31] microwave,[32] and radio frequency capacitively coupled (CCP) plasmas.[33] Control of NC size was achieved through plasma chemistry and residence time in the plasma. Figure 1.4 shows the

relationship between residence time and average grain size.[30] These reactors have been able to produce high-quality freestanding NCs that are ideal for manipulation and studying NC properties and devices.

This has led to interest in synthesizing other materials with nonthermal plasmas. Germanium is an obvious choice since its properties are fairly close to Si. Additionally Ge has a smaller bandgap and larger Bohr exciton radius than Si, leading to a stronger quantum confinement effect.[34] Germanium NCs have been synthesized with nonthermal plasmas in a fashion similar to Si NCs. Germanium NCs have been synthesized in an ICP reactor[31] and flow-through CCP reactor.[35] It was shown that alloys of Si_xGe_{x-1} NCs could also be synthesized in a CCP reactor.[36] This generated questions about whether compound semiconductors could be synthesized in a nonthermal plasma. Chapter 2 will show that it is possible to synthesize InP NCs with a flow-through nonthermal plasma.

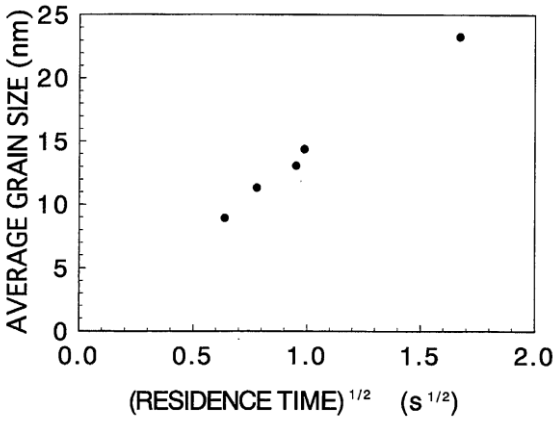

Figure 1.4: Si NCs average particle size as a function of the square-root of the residence time in a VHF plasma. Reproduced from reference 30.

1.5 Doped NCs

Doping, the intentional inclusion of impurities into semiconductors, was vital to the success of the semiconductor industry in developing integrated circuits.[37] While NCs exhibit size-dependent electrical and optical properties, the inclusion of dopants would further allow the tailoring of these properties. Doped NCs have the potential to independently control both size- and dopant-dependent properties. However, doping has remained a challenge for many NCs materials to date, specifically with II-VI NCs.[38] II-VI systems have had limited success with Mn doping.[39, 40]

Successful doping of silicon NCs seems to be less complicated. Fujii and co-workers demonstrated the incorporation of dopants into Si NCs embedded in an oxide matrix.[41, 42] More recently, plasma synthesized Si NCs have shown evidence of dopant incorporation using microwave[43, 44] and RF plasmas.[45] Little is known about the dopant-dependent properties of NCs, specifically with regard to the electronic properties of NC films. Si NCs with P or B dopants which have been sintered by laser have shown high conductivities.[43] Chemically doped PbSe NCs have shown properties with high mobilities and device quality behavior.[46, 47] Chapter 3 will discuss the electronic properties of P-doped Si NC films.

1.6 Bibliography

(1) Brus, L. Quantum crystallites and nonlinear optics. *Applied Physics A: Materials Science & Processing* **1991**, *53*, 465-474.

(2) Alivisatos, A. P. Semiconductor Clusters, Nanocrystals, and Quantum Dots. *Science* **1996**, 271, 933-937.
(3) Nozik, A. J. Quantum dot solar cells. *Physica E: Low-dimensional Systems and Nanostructures* **2002**, 14, 115-120.
(4) Han, M.; Gao, X.; Su, J. Z.; Nie, S. Quantum-dot-tagged microbeads for multiplexed optical coding of biomolecules. *Nat. Biotech.* **2001**, 19, 631-635.
(5) Coe, S.; Woo, W.; Bawendi, M.; Bulovic, V. Electroluminescence from single monolayers of nanocrystals in molecular organic devices. *Nature* **2002**, 420, 800-803.
(6) Selmarten, D.; Jones, M.; Rumbles, G.; Yu, P.; Nedeljkovic, J.; Shaheen, S. Quenching of Semiconductor Quantum Dot Photoluminescence by a π-Conjugated Polymer. *J. Phys. Chem. B* **2005**, 109, 15927-15932.
(7) Bawendi, M. G.; Wilson, W. L.; Rothberg, L.; Carroll, P. J.; Jedju, T. M.; Steigerwald, M. L.; Brus, L. E. Electronic structure and photoexcited-carrier dynamics in nanometer-size CdSe clusters. *Phys. Rev. Lett.* **1990**, 65, 1623-1626.
(8) Bawendi, M. G.; Carroll, P. J.; Wilson, W. L.; Brus, L. E. Luminescence properties of CdSe quantum crystallites: Resonance between interior and surface localized states. *J. Chem. Phys.* **1992**, 96, 946-954.
(9) Murray, C. B.; Norris, D. J.; Bawendi, M. G. Synthesis and characterization of nearly monodisperse CdE (E = sulfur, selenium, tellurium) semiconductor nanocrystallites. *J. Am. Chem. Soc.* **1993**, 115, 8706-8715.
(10) Micic, O. I.; Curtis, C. J.; Jones, K. M.; Sprague, J. R.; Nozik, A. J. Synthesis and Characterization of InP Quantum Dots. *J. Phys. Chem.* **1994**, 98, 4966-4969.
(11) Micic, O. I.; Sprague, J. R.; Curtis, C. J.; Jones, K. M.; Machol, J. L.; Nozik, A. J.; Giessen, H.; Fluegel, B.; Mohs, G.; Peyghambarian, N. Synthesis and Characterization of InP, GaP, and GaInP2 Quantum Dots. *J. Phys. Chem.* **1995**, 99, 7754-7759.
(12) Battaglia, D.; Peng, X. Formation of High Quality InP and InAs Nanocrystals in a Noncoordinating Solvent. *Nano Lett.* **2002**, 2, 1027-1030.
(13) Micic, O. I.; Sprague, J.; Lu, Z.; Nozik, A. J. Highly efficient band-edge emission from InP quantum dots. *Appl. Phys. Lett.* **1996**, 68, 3150-3152.
(14) Talapin, D. V.; Gaponik, N.; Borchert, H.; Rogach, A. L.; Haase, M.; Weller, H. Etching of Colloidal InP Nanocrystals with Fluorides: Photochemical Nature of the Process Resulting in High Photoluminescence Efficiency. *J. Phys. Chem. B* **2002**, 106, 12659-12663.
(15) Xie, R.; Battaglia, D.; Peng, X. Colloidal InP Nanocrystals as Efficient Emitters Covering Blue to Near-Infrared. *J. Am. Chem. Soc.* 2007, 129, 15432-15433.
(16) Xu, S.; Kumar, S.; Nann, T. Rapid Synthesis of High-Quality InP Nanocrystals. *J. Am. Chem. Soc.* **2006**, 128, 1054-1055.

(17) Li, L.; Reiss, P. One-pot Synthesis of Highly Luminescent InP/ZnS Nanocrystals without Precursor Injection. *J. Am. Chem. Soc.* **2008**, 130, 11588-11589.
(18) Pratsinis, S. E. Flame aerosol synthesis of ceramic powders. *Prog. Energ. Combust.* **1998**, 24, 197-219.
(19) Littau, K. A.; Szajowski, P. J.; Muller, A. J.; Kortan, A. R.; Brus, L. E. A luminescent silicon nanocrystal colloid via a high-temperature aerosol reaction. *J. Phys. Chem.* **1993**, 97, 1224-1230.
(20) Lewis, K. E.; Golden, D. M.; Smith, G. P. Organometallic bond dissociation energies: laser pyrolysis of iron pentacarbonyl, chromium hexacarbonyl, molybdenum hexacarbonyl, and tungsten hexacarbonyl. *J. Am. Chem. Soc.* **1984**, 106, 3905-3912.
(21) Stoldt, C. R.; Haag, M. A.; Larsen, B. A. Preparation of freestanding germanium nanocrystals by ultrasonic aerosol pyrolysis. *Appl. Phys. Lett.* **2008**, 93, 043125.
(22) Chen, X.; Mao, S. S. Titanium Dioxide Nanomaterials: Synthesis, Properties, Modifications, and Applications. *Chem. Rev.* **2007**, 107, 2891-2959.
(23) Goree, J. Charging of particles in a plasma. *Plasma Sources Sci. T.* 1994, 3, 400-406.
(24) Daugherty, J. E.; Porteous, R. K.; Graves, D. B. Electrostatic forces on small particles in low-pressure discharges. *J. Appl. Phys.* **1993**, 73, 1617-1620.
(25) Selwyn, G. S.; Singh, J.; Bennett, R. S. In situ laser diagnostic studies of plasma-generated particulate contamination. *J. Vac. Sci. Technol. A* **1989**, *7*, 2758-2765.
(26) Bouchoule, A.; Plain, A.; Boufendi, L.; Blondeau, J. P.; Laure, C. Particle generation and behavior in a silane-argon low-pressure discharge under continuous or pulsed radio-frequency excitation. *J. Appl. Phys.* **1991**, *70*, 1991-2000.
(27) Boufendi, L.; Bouchoule, A. Particle nucleation and growth in a low-pressure argon-silane discharge. *Plasma Sources Sci. T.* **1994**, *3*, 262-267.
(28) Canham, L. T. Silicon quantum wire array fabrication by electrochemical and chemical dissolution of wafers. *Appl. Phys. Lett.* **1990**, *57*, 1046-1048.
(29) Otobe, M.; Kanai, T.; Ifuku, T.; Yajima, H.; Oda, S. Nanocrystalline silicon formation in a SiH4 plasma cell. *J. Non-Cryst. Solids* **1996**, *198-200*, 875-878.
(30) Ifuku, T.; Otobe, M.; Oda, A. I. A. S. Fabrication of Nanocrystalline Silicon with Small Spread of Particle Size by Pulsed Gas Plasma. *Jpn. J. Appl. Phys.* **1997**, *36*, 4031-4034.
(31) Gorla, C. R.; Liang, S.; Tompa, G. S.; Mayo, W. E.; Lu, Y. *Am. Vac. Soc.*; AVS: Philadelphia, Pennsylvania (USA), **1997**; Vol. 15, pp. 860-864.
(32) Knipping, J.; Wiggers H.; Rellinghaus, B.; Roth P.; Konjhodzic D.; Meier C. Synthesis of High Purity Silicon Nanoparticles in a Low Pressure Microwave Reactor. *J. Nanosci. and Nanotechnol.* **2004**, *4*, 1039-1044.
(33) Mangolini, L.; Thimsen, E.; Kortshagen, U. High-Yield Plasma Synthesis of Luminescent Silicon Nanocrystals. *Nano Lett.* **2005**, *5*, 655-659.

(34) Bostedt, C.; van Buuren, T.; Willey, T. M.; Franco, N.; Terminello, L. J.; Heske, C.; Moller, T. Strong quantum-confinement effects in the conduction band of germanium nanocrystals. *Appl. Phys. Lett.* **2004**, *84*, 4056-4058.
(35) Gresback, R.; Holman, Z.; Kortshagen, U. Nonthermal plasma synthesis of size-controlled, monodisperse, freestanding germanium nanocrystals. *Appl. Phys. Lett.* **2007**, *91*, 093119-3.
(36) Pi, X. D.; Kortshagen, U. Nonthermal plasma synthesized freestanding silicon–germanium alloy nanocrystals. *Nanotechnology* **2009**, *20*, 295602.
(37) Seeger, K. Semiconductor physics; Springer, **2004**.
(38) Erwin, S. C.; Zu, L.; Haftel, M. I.; Efros, A. L.; Kennedy, T. A.; Norris, D. J. Doping semiconductor nanocrystals. *Nature* **2005**, *436*, 91-94.
(39) Norris, D. J.; Yao, N.; Charnock, F. T.; Kennedy, T. A. High-Quality Manganese-Doped ZnSe Nanocrystals. *Nano Lett.* **2001**, *1*, 3-7.
(40) Bhargava, R. N.; Gallagher , D.; Hong, X.; Nurmikko, A. Optical properties of manganese-doped nanocrystals of ZnS. *Phys. Rev. Lett.* **1993**, *72*, 416-419.
(41) Fujii, M.; Mimura, A.; Hayashi, S.; Yamamoto, K. Photoluminescence from Si nanocrystals dispersed in phosphosilicate glass thin films: Improvement of photoluminescence efficiency. *Appl. Phys. Lett.* **1999**, *75*, 184-186.
(42) Kanzawa, Y.; Fujii, M.; Hayashi, S.; Yamamoto, K. Doping of B atoms into Si nanocrystals prepared by rf cosputtering. *Solid State Commun.* **1996**, *100*, 227-230.
(43) Lechner, R.; Stegner, A. R.; Pereira, R. N.; Dietmueller, R.; Brandt, M. S.; Ebbers, A.; Trocha, M.; Wiggers, H.; Stutzmann, M. Electronic properties of doped silicon nanocrystal films. *J. Appl. Phys.* **2008**, *104*, 053701-7.
(44) Stegner, A. R.; Pereira, R. N.; Lechner, R.; Klein, K.; Wiggers, H.; Stutzmann, M.; Brandt, M. S. Doping efficiency in freestanding silicon nanocrystals from the gas phase: Phosphorus incorporation and defect-induced compensation. *Phys. Rev. B* **2009**, *80*, 165326.
(45) Pi, X. D.; Gresback, R.; Liptak, R. W.; Campbell, S. A.; Kortshagen, U. Doping efficiency, dopant location, and oxidation of Si nanocrystals. *Appl. Phys. Lett.* **2008**, *92*, 123102-3.
(46) Wehrenberg, B. L.; Yu, D.; Ma, J.; Guyot-Sionnest, P. Conduction in Charged PbSe Nanocrystal Films. *J. Phys. Chem. B* **2005**, *109*, 20192-20199.
(47) Talapin, D. V.; Murray, C. B. PbSe Nanocrystal Solids for n- and p-Channel Thin Film Field-Effect Transistors. *Science* **2005**, *310*, 86-89.

Chapter 2

2.1 Chapter overview

This chapter concerns a new method to synthesize indium phosphide nanocrystals using a nonthermal plasma. The plasma parameters are presented which yield nanocrystals with mean sizes between ~2-5 nm. The optical properties are studied as a function of plasma residence time. A liquid phase route is presented to increase the photoluminescence quantum yield through the growth of a ZnS shell. Appendix A highlights some efforts to use these nanocrystals in hybrid devices with P3HT.

2.2 Outline

Indium phosphide nanocrystals (InP NCs) have been synthesized with a scalable, flow-through, nonthermal plasma. Nanocrystal size is controlled through plasma operating parameters, where the residence time of the gas in the plasma region strongly influences the NC size. InP NCs ~2-5 nm in size have been synthesized with mass yields of 10-40 mg/hour. A size distribution of less than 20% the standard deviation of the mean nanocrystals size was achieved without size selection. Photoluminescence with quantum yields as high as 15% were observed when a shell of zinc sulfur (ZnS) was grown around the InP core to form a InP/ZnS core-shell structure.

2.3 Background

Semiconductor nanocrystals (NCs) have received increasing attention during the past 10-20 years due to their unique properties. They provide a wide range of flexibility through tunable size, high surface-to-volume ratios, and a variety of surface chemistries. These properties have led to the development of a new generation of materials and devices. Semiconductor NCs exhibit unique optical and electronic properties due to confinement of electronic carriers, the quantum confinement effect.[1, 2] Early work on NCs has focused on II-VI systems due to the relative ease of synthesizing high quality material using colloidal techniques.[1, 3, 4] Comparable synthesis methods for InP require days to produce quality material.[5, 6] More recently, synthesis of high quality InP NCs has been achieved with non-coordinating solvents[7] and weak coordinating solvents.[8] However, these methods still offer challenges for producing devices due to the electrically insulating organics attached to the NCs used for synthesis and stabilization.

Synthesis of NCs using nonthermal plasmas has become a viable method even for materials that have proven difficult to synthesize, such as Si[9, 10] and Ge.[11] An added advantage to plasma synthesis as compared to liquid phase routes is that the resulting material is free of ligands or surfactants. This makes integration of materials into devices easier, as it eliminates intermediate steps like ligand exchanges. Here we propose a method to synthesize InP NCs with a nonthermal plasma. Additionally, we show that typical solution chemistry can be used to grow a ZnS shell around a plasma synthesized InP NC core.

2.4 Experimental

Indium phosphide NCs were synthesized using a nonthermal radio-frequency (13.56 MHz) plasma operated at 2.5 Torr with 50-80 Watts of nominal power applied through a matching network. A system schematic can be seen in Figure 2.2. The reactor consists of 2 ring electrodes around a 3/8" OD quartz tube with a 1/4" ID. Similar reactor designs have been reported for synthesis of Si[9] and Ge NCs[11]. The ground and powered electrodes were located 3 and 4 cm, respectively, from the grounded metal fitting. 15% phosphine (PH_3) gas in hydrogen (H_2) and trimethylindium (TMIn, $In(CH_3)_3$) vapor were used as the phosphorus and indium precursors. Trimethylindium sublimes at room temperature allowing its vapor to be entrained in argon carrier gas.[12] Additional argon is used to sustain the plasma and dilute the precursors. This work used a ratio of 90 Ar : 17 H_2 : 3 PH_3 : 1 TMIn by mass, with total mass flow rates varied between 34-172 standard cubic centimeters per minute (sccm), which resulted in plasma residence times between 2-10 ms.

The precursors are dissociated in the plasma followed by nucleation and growth of InP NCs. The NCs are transported out of the plasma region by gas drag and deposited on a stainless steel mesh as a dry powder. The powder is extremely sensitive to air exposure; therefore all processes must be done with the exclusion of oxygen and moisture. After synthesis, the material is transferred under nitrogen to a glove box or Schlenk line for handling and reactions. NCs produced in the plasma reacted readily with ligands and

coordinating solvents such as amines, phosphine oxides, and fatty acids in the presence of non-coordinating solvents at temperatures less than 200 ^{o}C in less than one hour.

The ZnS shells were grown as follows: a known mass of dry InP nanocrystals was transferred into a solution of octadecene (ODE) and myristic acid, then the solution was sonicated for 5 minutes and heated to 200 ^{o}C for 30 minutes under a flow of nitrogen. Each monolayer of ZnS was grown by using preheated solutions of 0.05 M zinc stearate in ODE and sulfur in ODE. The zinc and sulfur precursors were injected separately at 15 minute intervals with stoichiometric ratios (based on spherical volume thickness calculation) and heated to 220 ^{o}C. The solution was then cooled and repeatedly washed by centrifugation and precipitation. The InP/ZnS NCs were then re-dissolved in toluene.

Transmission electron microscopy (TEM) was performed by dropping a small amount of colloid onto a thin carbon coated TEM grid. A FEI Tecnai T12 operated at 120 kV was used. X-ray diffraction (XRD) was performed on a Bruker-AXS Microdiffractometer with 2.2 kW sealed Cu X-ray Source. Raman spectroscopy was performed on a Witec Alpha300R confocal raman microscope. Samples for XRD and Raman were prepared by drop casting concentrated solution onto glass substrates. Photoluminescence (PL) measurements were preformed on a Photon Technology International QuantaMaster 40 UV Vis spectrofluorometer. UV-Vis absorption measurements were performed with an Ocean Optics spectrometer (HR2000) using a combination of deuterium and tungsten halogen lamps (DH-2000-BALL).

2.5 Results and Discussion

Bare InP NCs oxidize rapidly making characterization of dry powder difficult. Ligands are used to inhibit oxidation, afford solubility, and to allow for characterization. Figure 2.3 shows a TEM image of InP NCs synthesized with a 10 ms residence time and passivated with myristic acid. The (111) lattice fringes are clearly visible in several NCs. The inset in Figure 2.3 shows a selected area diffraction (SAD) pattern with the rings of the (111), (220), and (311) InP planes clearly present. The average NC size determined by counting >50 particles was 4.3 nm with a standard deviation of 0.8 nm. Size distribution is large compared to liquid phase synthesis techniques, where less than 10% is common;[13] however it is a narrow distribution for gas phase synthesized NCs.[14]

Raman spectroscopy and XRD were used to further investigate the NC properties. Figure 2.4 shows an XRD spectrum of NCs synthesized with a residence time of 6 ms. The (111), (220) and (311) peaks are clearly visible with a small signal from the (200) peak. This confirms the presence of InP with a zinc-blend structure. Debye-Scherrer broadening gives a NC size of 3.4 nm, while TEM results found a slightly large mean size of 3.8 nm. The Raman spectrum in Figure 2.5 shows InP NCs synthesized with residence times of 4, 6, and 10 ms and passivated with myristic acid. The peak of the longitudinal optical (LO) mode decreases while the transverse optical (TO) mode increases as residence time and NC size decreases. This was also observed by Guzelian et al. and was thought to be due to a loss of symmetry as NC size decreases.[15]

UV-Vis absorption was performed on colloidal InP NCs with myristic acid as the ligand after being heated to 190 °C for 1 hour. Figure 2.6 shows that the onset of the absorption changes as a function of the residence time of the NCs in the plasma. Shorter residence times lead to a blue shift in the onset of the absorption. The first exciton peak is not clear due to the broad size distribution. The onset of the absorption correlates well with sizes observed in TEM.

Both as-produced and passivated NCs with ligands show little or no PL. NCs that were allowed to oxidize exhibit a small increase in PL, however the quantum yield (QY) of these samples was still less than 1%. Low QY in InP NCs is often attributed to phosphorus dangling bonds at the surface, which lead to non-radiative recombination of photogenerated carriers.[16] Several methods have been introduced to eliminate non-radiative recombination sites including the use of fluorine etches[16] and capping with a wideband gap semiconductor such as ZnS.[13] For this work, we used the method of growing a ZnS layer. Figure 2.7 shows representative PL spectra of several samples of InP/ZnS core-shell NCs. Peak emission from the InP/ZnS NCs varies from 508 to 635 nm with the full-width half-maximum (FWHM) of the PL varying between 70 and 100 nm. The peak emission, like the absorption onset, is strongly dependent on the residence times of the NCs in the plasma. Figure 2.8 shows the relationship between the residence time and peak emission. Unfortunately, due to experimental setup limitations a wider range of residence times could not be explored. However there appears to be no

indication that a continuous range of emission from bulk emission at 1.37 eV to quantum confined NC emission at 2.5 eV could not be achieved.

Quantum yields of 10-15% were measured for InP/ZnS structures; we credit this relatively low value to the use of our Zn and S precursors of zinc stearate and elemental sulfur. It is more common to use the volatile precursors of diethylzinc and bis(trimethylsilyl) sulfide.[17] We believe that if these more volatile precursors were used, the QYs would be comparable to other NC systems.

2.6 Conclusion

In summary, InP NCs with controllable size were successfully synthesized from a flow-through nonthermal plasma. Size control was achieved through adjusting the residence time of NCs in the plasma. This synthesis process yields NCs which are bare and free-standing, which may simplify device integration. Additionally we have found that these NCs can easily form a colloid with a variety of ligands and then techniques developed for colloidal systems can be used. When a ZnS shell is grown around the InP core, QYs of 10-15% were observed. This work demonstrates that it is possible to synthesize compound semiconductor NCs with a plasma, opening up the possibility of a wider range of plasma-synthesized NC materials.

Figure 2.1: Photograph of InP/ZnS core/shell NCs illiuminated by a UV lamp.

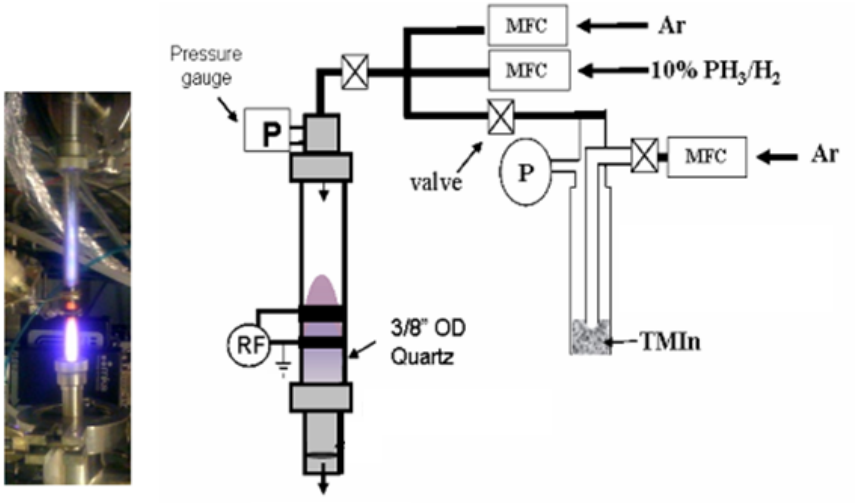

Figure 2.2: Nonthermal plasma synthesis of InP NCs. (left) Photograph and (right) schematic representation.

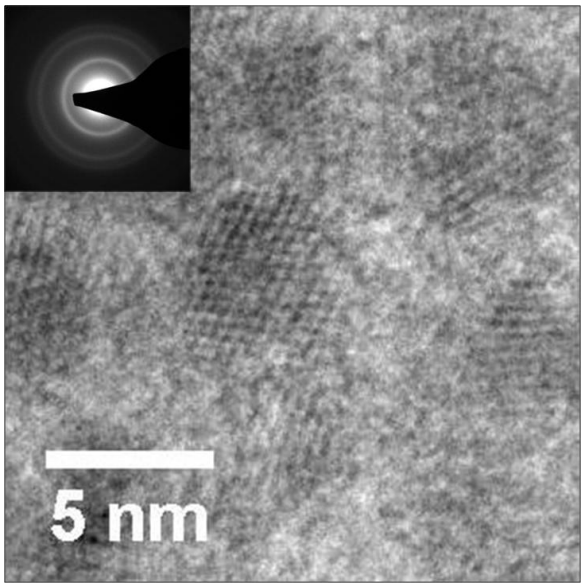

Figure 2.3: TEM image of InP NCs synthesized with 10 ms residence time. The average size is 4.3 nm. Inset: SAD showing (111), (220) and (311) planes.

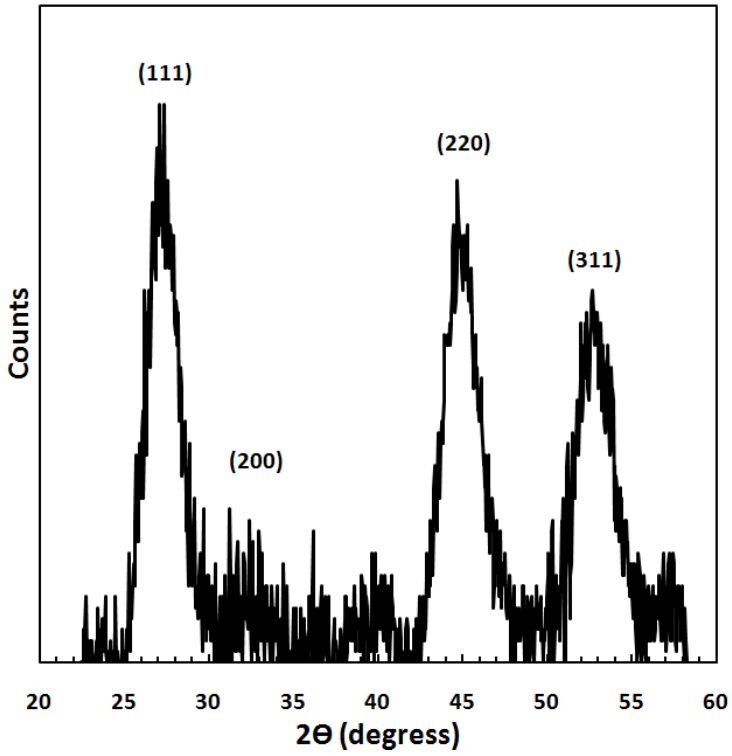

Figure 2.4: XRD spectrum of InP NCs synthesized with 6 ms residence time. The Debye-Scherrer size is 3.6 nm.

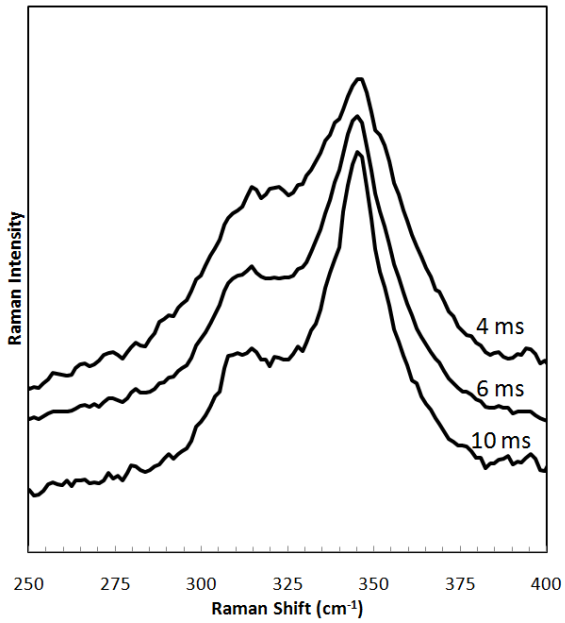

Figure 2.5: Raman spectra of InP NCs passivated with myristic acid synthesized with various plasma residence times.

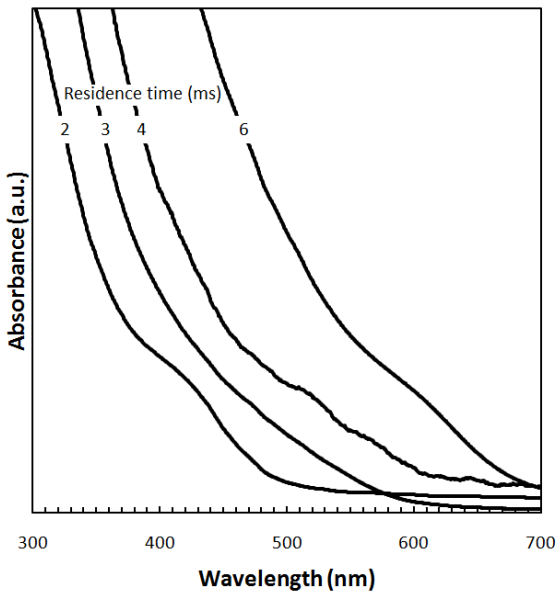

Figure 2.6: UV-Vis absorption spectra of InP NCs passivated with myristic acid synthesized with various residence times in the plasma.

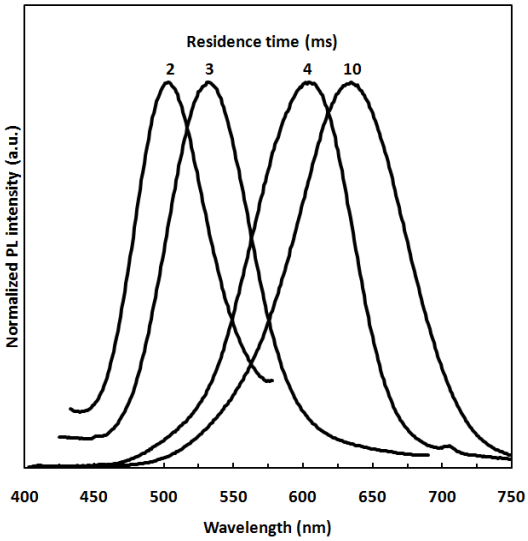

Figure 2.7: Representative PL spectra of InP/ZnS core/shell NCs synthesized with various plasma residence times

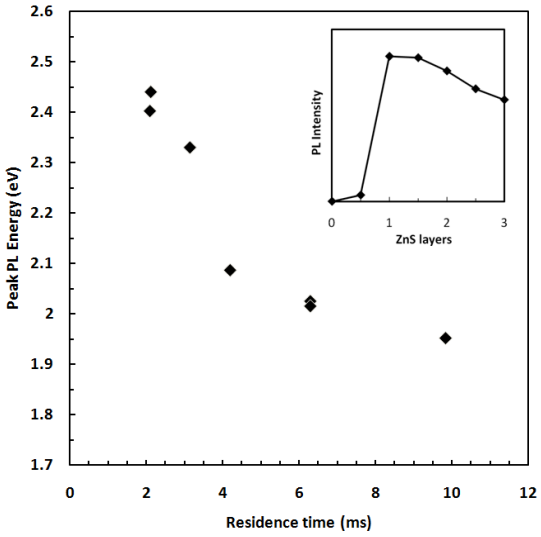

Figure 2.8: Effect of plasma residence time on peak PL emission from InP/ZnS core/shell structures. Inset: Layer by layer effect of ZnS growth on PL intensity.

2.7 Bibliography

(1) Murray, C. B.; Norris, D. J.; Bawendi, M. G. Synthesis and characterization of nearly monodisperse CdE (E = sulfur, selenium, tellurium) semiconductor nanocrystallites. *J. Am. Chem. Soc.* **1993**, *115*, 8706-8715.

(2) Efros, A.; Rosen, M.; Kuno, M.; Nirmal, M.; Norris, D.; Bawendi, M. Band-edge exciton in quantum dots of semiconductors with a degenerate valence band: Dark and bright exciton states. *Phys. Rev. B* **1996**, *54*, 4843-4856.

(3) Hines, M. A.; Guyot-Sionnest, P. Synthesis and Characterization of Strongly Luminescing ZnS-Capped CdSe Nanocrystals. *J. Phys. Chem.* **1996**, *100*, 468-471.

(4) Peng, X.; Schlamp, M. C.; Kadavanich, A. V.; Alivisatos, A. P. Epitaxial Growth of Highly Luminescent CdSe/CdS Core/Shell Nanocrystals with Photostability and Electronic Accessibility. *J. Am. Chem. Soc.* **1997**, *119*, 7019-7029.

(5) Micic, O. I.; Curtis, C. J.; Jones, K. M.; Sprague, J. R.; Nozik, A. J. Synthesis and Characterization of InP Quantum Dots. *J. Phys. Chem.* **1994**, *98*, 4966-4969.

(6) Micic, O. I.; Sprague, J. R.; Curtis, C. J.; Jones, K. M.; Machol, J. L.; Nozik, A. J.; Giessen, H.; Fluegel, B.; Mohs, G.; Peyghambarian, N. Synthesis and Characterization of InP, GaP, and GaInP2 Quantum Dots. *J. Phys. Chem.* **1995**, *99*, 7754-7759.

(7) Battaglia, D.; Peng, X. Formation of High Quality InP and InAs Nanocrystals in a Noncoordinating Solvent. *Nano Lett.* **2002**, *2*, 1027-1030.

(8) Xu, S.; Kumar, S.; Nann, T. Rapid Synthesis of High-Quality InP Nanocrystals. *J. Am. Chem. Soc.* **2006**, *128*, 1054-1055.

(9) Mangolini, L.; Thimsen, E.; Kortshagen, U. High-Yield Plasma Synthesis of Luminescent Silicon Nanocrystals. *Nano Lett.* **2005**, *5*, 655-659.

(10) Knipping, J.; Wiggers H.; Rellinghaus, B.; Roth P.; Konjhodzic D.; Meier C. Synthesis of High Purity Silicon Nanoparticles in a Low Pressure Microwave Reactor. *J. Nanosci. and Nanotechnol.* **2004**, *4*, 1039-1044.

(11) Gresback, R.; Holman, Z.; Kortshagen, U. Nonthermal plasma synthesis of size-controlled, monodisperse, freestanding germanium nanocrystals. *Appl. Phys. Lett.* **2007**, *91*, 093119-3.

(12) Shenai-Khatkhate, D. V.; DiCarlo Jr., R. L.; Ware, R. A. Accurate vapor pressure equation for trimethylindium in OMVPE. *J. Cryst. Growth* **2008**, *310*, 2395-2398.

(13) Xie, R.; Battaglia, D.; Peng, X. Colloidal InP Nanocrystals as Efficient Emitters Covering Blue to Near-Infrared. *J. Am. Chem. Soc.* **2007**, *129*, 15432-15433.

(14) Kruis, F. E.; Fissan, H.; Peled, A. Synthesis of nanoparticles in the gas phase for electronic, optical and magnetic applications--a review. *J. Aerosol Sci.* **1998**, *29*, 511-535.

(15) Guzelian, A. A.; Katari, J. E. B.; Kadavanich, A. V.; Banin, U.; Hamad, K.; Juban, E.; Alivisatos, A. P.; Wolters, R. H.; Arnold, C. C.; Heath, J. R. Synthesis of Size-

Selected, Surface-Passivated InP Nanocrystals. *J. Phys. Chem.* **1996**, *100*, 7212-7219.
(16) Talapin, D. V.; Gaponik, N.; Borchert, H.; Rogach, A. L.; Haase, M.; Weller, H. Etching of Colloidal InP Nanocrystals with Fluorides: Photochemical Nature of the Process Resulting in High Photoluminescence Efficiency. *J Phys. Chem. B* **2002**, *106*, 12659-12663.
(17) Langof, L.; Fradkin, L.; Ehrenfreund, E.; Lifshitz, E.; Micic, O.; Nozik, A. Colloidal InP/ZnS core-shell nanocrystals studied by linearly and circularly polarized photoluminescence. *Chem. Phys.* **2004**, *297*, 93-98.

Chapter 3

3.1 Chapter overview

This chapter concerns the properties of P-doped silicon nanocrystal films. Doped NCs were synthesized in a nonthermal plasma. Films were made by spin casting suspensions of NCs onto glass substrates. The conductivity was studied as a function of the nominal doping concentration from 0-10^{-1} dopants per silicon atoms. Conductivities of highly doped films were found to be up to 10^{-1} S/cm.

3.2 Outline

Doped silicon nanocrystals (Si NCs) are of interest for optical and electronic device applications because their optical and electronic properties may be tuned by controlling NC size and dopant concentration. This manuscript describes a method to deposit doped Si NCs films and the results of electrical characterization on these films. Phosphorus-doped Si NCs have been synthesized with a nonthermal plasma, yielding NCs with mean sizes from 8-13 nm. Films were created by spin casting suspensions of Si NCs in 1,2-dichlorobenzene onto glass substrates with predeposited aluminum electrodes to study electrical conductivity as a function of dopant concentration. A continuous range of conductivities from 10^{-11} to 10^{-1} S/cm were observed for nominal atomic doping concentrations from 0 to 10^{-1} dopants per Si atoms.

3.3 Introduction

Doping, the intentional inclusion of impurities, has been vital to the success of the semiconductor device industry. Recently, doping of semiconductor nanocrystals (NCs) has received significant attention. However many challenges still remain, including developing methods and materials which are suitable for doping of NCs.[1] There are several ideas on why incorporation of dopants into NCs in challenging. Self-purification has been proposed, where energetics force dopants to the surface.[2] Others have proposed that surface morphology, NC shape, and growth chemistry are the main factors determining dopant incorporation.[1] To date, incorporation of dopants into NCs using colloidal techniques has been limited to a small number of materials and dopants.[3,4,5, 6,7,8] These materials contain rare**,** toxic materials leading to concerns about large scale applications. These concerns have led to interest in using more abundant and non-toxic materials such as silicon (Si).[9] Silicon NCs embedded in an oxide matrix have exhibited doping-dependent behavior.[10, 11]More recently, free-standing doped Si NCs have been synthesized in the gas phase using plasmas.[12, 13]

Additional attention has focused on techniques for depositing films of NCs from solution which enable low-cost methods for producing large area thin-film optical and electronic devices. The advantage of NC films is the ability to tune their optical and electronic properties through the size of the constituent NCs while still providing a continuous pathway for charge carriers.

We have previously reported a method to synthesize bare free-standing Si NCs in a nonthermal plasma.[14] By introducing phosphine (PH_3) or diborane (B_2H_6) into the precursor stream we have also shown that dopants are incorporated into the NCs.[13] Through careful solvent choice these NCs can form a stable suspension in 1,2-dichlorobenzene (DCB). Here the dopant-dependent electrical properties are studied for NC films created by spin casting non-functionalized doped Si NCs.

3.4 Experimental

Phosphorus-doped Si NCs were synthesized with a nonthermal flow-through RF (13.56 MHz) plasma. The reactor consists of a 1" OD quartz tube with two copper ring electrodes. Similar reactors have been described previously.[13, 14] For all samples (unless otherwise noted) Si NCs were synthesized using 70 and 2 standard cubic centimeters per minute (sccm) of argon and silane, respectively, with a varying amount of PH_3 (from $2x10^{-5}$-0.2 sccm) to adjust the doping level. The plasma was operated at 2.5-3 Torr and 180 W of nominal power through a matching network. Samples were collected on a stainless steel mesh between two gate valves used to transport samples to a glovebox. DCB (ACROS) was added to a vial containing the stainless steel mesh with a measured mass of NCs until the concentration reached 8-10 mg/ml, and the suspension was sonicated for at least 5 mins. The mesh was removed and the suspension was again sonicated. Directly after sonication, a few drops of the suspension were spun at 700 rpm for 1 minute onto glass substrates with pre-deposited aluminum contacts. The contacts

were deposited by evaporation of 100 nm of aluminum with a gap of 100 μm and a width of 1 mm. The samples were allowed to dry completely which happened in less than 1 hour, leaving a barely visible Si NC film.

The spin-coated Si NCs films were then annealed at 400 °C for 30 minutes on a hotplate in a glovebox, unless otherwise noted, to form ohmic contacts with the pre-deposited aluminum contacts. Samples were then controllably cooled and conductivity measurements were taken at 25-50 degree increments. The conductivity was determined from current-voltage (I-V) characteristics in which the applied voltage was swept between -20 and 20 VDC. All preparation and electrical measurements on the NC films were done under a nitrogen atmosphere.

Transmission electron microscopy (TEM) was used to determine NC size and shape. X-ray diffraction (XRD) and Raman spectroscopy were used to confirm TEM analysis. A scanning electron microscope (SEM) was used to determine fill morphology and coverage; charging was reduced by sputtering a 50 Å layer of platinum over the Si NC film.

3.5 Results and Discussion

Under the conditions specified in the experimental section, Si NCs with a mean diameter between 8-13 nm were synthesized with size distributions less than 25% of the mean sizes. The mean sizes are consistent in both TEM measurements and Debye-Scherrer broadening in XRD. Figure 3.1 shows TEM images of spin cast Si NC films

unheated and heated to 400 °C that were scraped off glass substrates and transferred to TEM grids. When Si NCs were heated to 400 °C, there was no observable change in size, shape, or crystallinity, although there is most likely a change in the surface chemistry, including the loss of SiH_3 and SiH_2. It was shown by Holm and Roberts that sintering of Si NCs does not occur until temperatures greater than 500 °C are reached.[15] From TEM analysis and the results of Holm and Roberts, it is reasonable to assume that no drastic changes in the NC structure occurred due to heating to 400 C.

Spin cast films consist of densely packed NCs with zero to several monolayers thick along with agglomerates that can reach up to 100s of nm in size. In Figure 3.2a an SEM image shows a nearly continuous section of film with some pinholes. The edge of the aluminum electrode is visible under the film. Figure 3.2b shows a higher magnifaction image, where densely packed individual Si NCs of one to several monolayers and pinholes are evident.

Figure 3.3 shows I-V characteristics for a nominal P-doped $5x10^{-2}$ dopants per Si atom Si NC film after it has been heated to 400 °C and incremental traces cooling to 55 °C. The inset shows the extracted conductivity of the same sample as it is ramped from room temperature to 400 °C and cooled. From the inset, we see a significant increase in conductivity after annealing. We believe the higher conductivities after annealing were the result of two effects. The first effect is a change in the surface chemistry of the Si NCs at temperatures of 175-350 °C which could eliminate dangling bonds and trap sites

for carriers.[15] The other effect is the formation of ohmic contacts between the aluminum and Si NC film; at temperatures below 400 °C during ramp-up non-linear I-V traces are observed indicating a Schottky barrier. Once samples are annealed to 400 °C I-V traces become linear, indicating there is ohmic contact between the Si NC film and the aluminum contacts.

The electrical conductivity of spin-cast Si NC films were studied as a function of the nominal doping level. The nominal doping level is determined by the atomic fraction of dopant introduced into the plasma. It was found that electrically active doping levels may be an order of magnitude less than nominal doping concentrations in plasma synthesized NCs.[13 16] Intrinsic NCs and NCs doped with a range of nominal phosphorus doping levels from 10^{-4} to 10^{-1} dopants per Si atoms along with intrinsic NCs were studied. Figure 3.4 shows the room temperature conductivity of Si NC films after annealing at 400 °C. The inset of Figure 3.4 shows example conductivities as a function of T^{-1} for several doping levels; there is Arrhenius-like behavior observed for all doping levels. Room temperature conductivities less than $5x10^{-6}$ S/cm have been extrapolated from fitting higher temperature conductivities due to resolution limitations of the source-meter. Room temperature conductivities of intrinsic Si NC films were found to be ~10^{-11} S/cm as the nominal doping level is increased to 0.1 dopants per Si atom a continuous range of conductivities is observed. At the highest nominal doping level of 0.1 dopants per Si atom, conductivities were found to be 10^{-3}-10^{-1} S/cm at room temperature. These

films can be compared to amorphous Si grown by plasma-enhanced chemical vapor deposition (PECVD) where a disordered atomic structure is characteristic of the film. A close analogy can be used for Si NC films, where order exists through the core of the NCs, while the surface and interface of the NCs is disordered. Conductivities for PECVD amorphous Si films of 10^{-10} to 10^{-9} S/cm are reported for intrinsic films, while P-doped amorphous Si films show conductivities up to 10^{-1} S/cm.[17] These values are similar to the values reported here.

3.6 Conclusion

This chapter has presented a method to synthesize electrically active doped Si NCs and electrical properties of doped Si NC films. A nonthermal plasma was employed to synthesize bare, free standing P-doped Si NCs with mean diameters between 8-13 nm and nominal P concentrations between 0 and 10^{-1} dopants per silicon atoms. Films with zero to several monolayers of NCs were formed by spin casting solutions of Si NCs in DCB with weight/volume concentrations of 8-10 mg/ml. A continuous range of conductivities from 10^{-11} to 10^{-1} S/cm were achieved by varying dopant concentration. The results presented have implications for optical and electronic devices, where control of dopant incorporation is vital for manipulation of the electrical properties of devices.

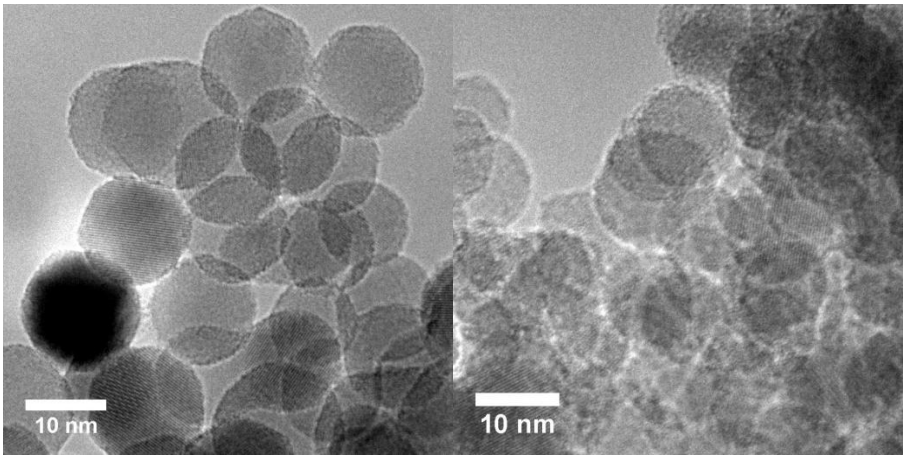

Figure 3.1: TEM images of Si NCs a) unheated and b) heated to 400 °C for 2 hours with no necking or sintering observed.

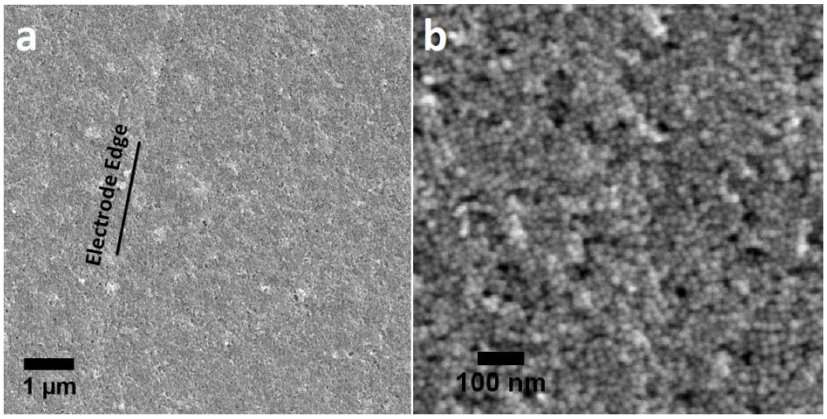

Figure 3.2: SEM images of Si NCs spin cast onto a glass substrate with pre-deposited aluminum contacts. a) Low magnification image showing underlying aluminum contact and b) a high magnification image showing individual NCs and pin-holes. Images courtesy of Zachary Holman.

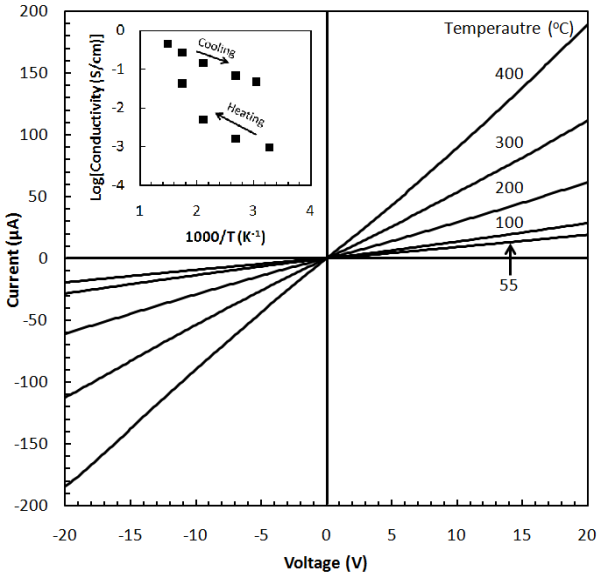

Figure 3.3: I-V traces of for temperatures between 55-400 C for a $5x10^{-2}$ dopants per silicon atoms P-doped Si NC film after it was heated to 400 °C. Inset: conductivity as a function of T^{-1}, showing the effect of annealing at 400 °C.

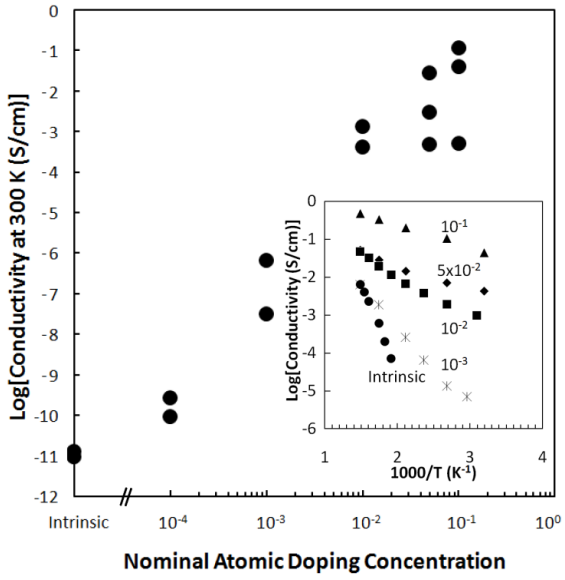

Figure 3.4: Room temperature conductivity of P-doped Si NC films annealed at 400 °C as a function of nominal atomic doping cocentration. Inset: example conductivities vs T^{-1} for various doping concentrations.

3.7 Bibliography

(1) Erwin, S. C.; Zu, L.; Haftel, M. I.; Efros, A. L.; Kennedy, T. A.; Norris, D. J. Doping semiconductor nanocrystals. *Nature* **2005**, 436, 91-94.

(2) Dalpian, G. M.; Chelikowsky, J. R. Self-Purification in Semiconductor Nanocrystals. *Phys. Rev. Lett.* **2006**, 96, 226802.

(3) Talapin, D. V.; Murray, C. B. PbSe Nanocrystal Solids for n- and p-Channel Thin Film Field-Effect Transistors. *Science* **2005**, 310, 86-89.

(4) Norris, D. J.; Yao, N.; Charnock, F. T.; Kennedy, T. A. High-Quality Manganese-Doped ZnSe Nanocrystals. *Nano Lett.* **2001**, 1, 3-7.

(5) Wehrenberg, B. L.; Yu, D.; Ma, J.; Guyot-Sionnest, P. Conduction in Charged PbSe Nanocrystal Films. *J. Phys. Chem. B* **2005**, 109, 20192-20199.

(6) Bhargava, R. N.; Gallagher, D.; Hong, X.; Nurmikko, A. Optical properties of manganese-doped nanocrystals of ZnS. *Phys. Rev. Lett.* **1993**, 72, 416-419.

(7) Du, H.; Chen, C.; Krishnan, R.; Krauss, T. D.; Harbold, J. M.; Wise, F. W.; Thomas, M. G.; Silcox, J. Optical Properties of Colloidal PbSe Nanocrystals. *Nano Lett.* **2002**, 2, 1321-1324.

(8) Hanif, K. M.; Meulenberg, R. W.; Strouse, G. F. Magnetic Ordering in Doped Cd1-xCoxSe Diluted Magnetic Quantum Dots. *J. Am. Chem. Soc.* **2002**, 124, 11495-11502.

(9) Borini, S.; Boarino, L.; Amato, G. Coulomb blockade sensors based on nanostructured mesoporous silicon. *Physica E* **2007**, 38, 197-199.

(10) Fujii, M.; Mimura, A.; Hayashi, S.; Yamamoto, K. Photoluminescence from Si nanocrystals dispersed in phosphosilicate glass thin films: Improvement of photoluminescence efficiency. *Appl. Phys. Lett.* **1999**, 75, 184-186.

(11) Lechner, R.; Stegner, A. R.; Pereira, R. N.; Dietmueller, R.; Brandt, M. S.; Ebbers, A.; Trocha, M.; Wiggers, H.; Stutzmann, M. Electronic properties of doped silicon nanocrystal films. *J. Appl. Phys.* **2008**, 104, 053701-7.

(12) Stegner, A. R.; Pereira, R. N.; Klein, K.; Lechner, R.; Dietmueller, R.; Brandt, M. S.; Stutzmann, M.; Wiggers, H. Electronic Transport in Phosphorus-Doped Silicon Nanocrystal Networks. *Phys. Rev. Lett.* **2008**, 100, 026803.

(13) Pi, X. D.; Gresback, R.; Liptak, R. W.; Campbell, S. A.; Kortshagen, U. Doping efficiency, dopant location, and oxidation of Si nanocrystals. *Appl. Phys. Lett.* **2008**, 92, 123102-3.

(14) Mangolini, L.; Thimsen, E.; Kortshagen, U. High-Yield Plasma Synthesis of Luminescent Silicon Nanocrystals. *Nano Lett.* **2005**, 5, 655-659.

(15) Holm, J.; Roberts, J. T. Sintering, Coalescence, and Compositional Changes of Hydrogen-Terminated Silicon Nanoparticles as a Function of Temperature. *J. Phys. Chem. C* **2009**, 113, 15955-15963.

(16) Stegner, A. R.; Pereira, R. N.; Lechner, R.; Klein, K.; Wiggers, H.; Stutzmann, M.; Brandt, M. S. Doping efficiency in freestanding silicon nanocrystals from the gas

phase: Phosphorus incorporation and defect-induced compensation. *Phys. Rev. B* **2009**, 80, 165326.
(17) Spear, W.; Le Comber, P. Substitutional doping of amorphous silicon. *Solid State Commun.* **1993**, 88, 1015-1018.

Chapter 4

4.1 Conclusion

This thesis reports on the development of plasma synthesis of InP NCs and on the properties of doped Si NCs films. These two areas represent significant progress in the fabrication of nanomaterial based devices. We demonstrate the controlled synthesis of free-standing InP NCs and we show these InP NCs can be used in wet chemical colloidal techniques. Additionally the growth of a shell of ZnS, using previously published colloidal technique, allows for a drastic improvement in the photoluminescence quantum yield. Emission from the blue-green to the red is observed when a ZnS shell is grown. This method offers great flexibility in the fabrication of devices. A wide variety of stabilizing ligands can be used if colloidal techniques are desired but also no ligands are required if carrier transport through networks of NCs is necessary. Some preliminary work on the development of InP/P3HT hybrid devices is reported in Appendix A.

The electronic properties of doped Si NC films are vital to the development of semiconductor NC devices. The work presented in this thesis demonstrates two important properties: (1) That films of NCs can be electrically conductive with conductivities up to 10^{-1} S/cm and (2) films of doped Si NCs show dopant-dependent conductivities. These results are not only important for basic understanding of doped NCs but also give an indication of the potential device quality achievable.

4.2 Future work

Doped Si NC films have great a potential to be used in a wide variety of next generation devices. Including transistors, photovoltaics, and light emitting diodes. To further understand the properties of doped Si NC films a variety of experiments can be used. In Chapter 3 the doping-dependent electrical properties were studied as a function of phosphorus doping level. These results can be expanded to include boron doped-Si NCs. Preliminary results indicate similar behavior with conductivities up to 10^{-2} S/cm for 10^{-2} boron dopants per silicon atom. A full study would point out the differences, if any, between n- and p-type Si NCs. Other important properties to study are the transport mechanisms and carrier mobilities.

Transport mechanisms can be studied using low temperature conductivities studies. A variety of mechanisms have been proposed for NC films: extended transport, percolation hopping,[1] Mott variable-range hopping (VRH),[2] Efros-Shklovskii (ES-VRH),[3] Fowler-Nordheim field emission tunneling,[4] and space charge limited current (SCLC).[5] Oda's group has studied the transport mechanism in intrinsic Si NCs and has reported SCLC behavior above 200 K, while below 200 K they observed either percolation or ES-VRH behavior. [6, 7]

Another property which is important to study is the mobilities of carriers. The effective electron and hole mobilities can be extracted from Hall effect measurements or through transistor's transfer curve. To determine the defect concentration and compensation by dopants, electron paramagnetic resonance (EPR) can be used.

An important experimental parameter to determine is the effect of contacts. While for our measurements we noticed the formation of ohmic contacts at temperatures of 400 °C, other effects could be causing increases in conductivity. The formation of ohmic contacts could be achieved through evaporation of contacts on top of the film, while in our previous work, contacts were pre-deposited.

Ultimately, the goal is to produce high quality devices. Kortshagen's group has already demonstrated the fabrication of hybrid solar cells[8] and hybrid LEDs (to be published) with intrinsic Si NCs. By introducing dopants into the NCs a wider variety of device configurations is possible. QD solar cells with multiple junctions of different NC size along with different doping profiles are possible. Incorporation of dopants into devices like hybrid solar cells may allow for the tuning of energy levels and a better carrier transport through the NC network.

4.3 Bibliography

(1) Simánek, E. The temperature dependence of the electrical resistivity of granular metals. *Solid State Commun.* **1981**, *40*, 1021-1023.
(2) Mott, N. Metal-Insulator Transition. *Rev. Mod. Phys.* **1968**, *40*, 677-683.
(3) Efros, A. L.; Shklovskii, B. I. Electronic Properties of Doped Semiconductors; Springer: Berlin, 1984.
(4) Fowler, R. H.; Nordheim, L. Electron Emission in Intense Electric Fields. *Proc. R. Soc. Lond. A* **1928**, *119*, 173-181.
(5) Lampert, M. A.; Many, A.; Mark, P. Space-Charge-Limited Currents Injected from a Point Contact. *Phys. Rev.* **1964**, *135*, A1444.
(6) Rafiq, M. A.; Tsuchiya, Y.; Mizuta, H.; Oda, S.; Uno, S.; Durrani, Z. A. K.; Milne, W. I. Charge injection and trapping in silicon nanocrystals. *Appl. Phys. Lett.* **2005**, *87*, 182101-3.

(7) Rafiq, M. A.; Tsuchiya, Y.; Mizuta, H.; Oda, S.; Uno, S.; Durrani, Z. A. K.; Milne, W. I. Hopping conduction in size-controlled Si nanocrystals. *J. Appl. Phys.* **2006**, *100*, 014303-4.
(8) Liu, C.; Holman, Z. C.; Kortshagen, U. R. Hybrid Solar Cells from P3HT and Silicon Nanocrystals. *Nano Lett.* **2009**, *9*, 449-452.

Bibliography

Alivisatos AP. 1996. Semiconductor Clusters, Nanocrystals, and Quantum Dots. *Science* 271(5251):933-937.

Battaglia D and Peng X. 2002. Formation of High Quality InP and InAs Nanocrystals in a Noncoordinating Solvent. *Nano Letters* 2(9):1027-1030.

Bawendi MG, Carroll PJ, Wilson WL, and Brus LE. 1992. Luminescence properties of CdSe quantum crystallites: Resonance between interior and surface localized states. *J. Chem. Phys.* 96(2):946-954.

Bawendi MG, Wilson WL, Rothberg L, Carroll PJ, Jedju TM, Steigerwald ML, and Brus LE. 1990. Electronic structure and photoexcited-carrier dynamics in nanometer-size CdSe clusters. *Phys. Rev. Lett.* 65(13):1623-1626.

Bhargava RN, Gallagher D, Hong X, and Nurmikko A. 1993. Optical properties of manganese-doped nanocrystals of ZnS. *Phys. Rev. Lett.* 72(3):416-419.

Borini S, Boarino L, and Amato G. 2007. Coulomb blockade sensors based on nanostructured mesoporous silicon. *Physica E: Low-dimensional Systems and Nanostructures* 38(1-2):197-199.

Bostedt C, van Buuren T, Willey TM, Franco N, Terminello LJ, Heske C, and Moller T. 2004. Strong quantum-confinement effects in the conduction band of germanium nanocrystals. *Appl. Phys. Lett.* 84(20):4056-4058.

Bouchoule A, Plain A, Boufendi L, Blondeau JP, and Laure C. 1991. Particle generation and behavior in a silane-argon low-pressure discharge under continuous or pulsed radio-frequency excitation. *J. Appl. Phys.* 70(4):1991-2000.

Boufendi L and Bouchoule A. 1994. Particle nucleation and growth in a low-pressure argon-silane discharge. *Plasma Sources Science and Technology* 3(3):262-267.

Brus L. 1991. Quantum crystallites and nonlinear optics. *Applied Physics A: Materials Science & Processing* 53(6):465-474.

Canham LT. 1990. Silicon quantum wire array fabrication by electrochemical and chemical dissolution of wafers. *Appl. Phys. Lett.* 57(10):1046-1048.

Chen X and Mao SS. 2007. Titanium Dioxide Nanomaterials: Synthesis, Properties, Modifications, and Applications. *Chemical Reviews* 107(7):2891-2959.

Coe S, Woo W, Bawendi M, and Bulovic V. 2002. Electroluminescence from single monolayers of nanocrystals in molecular organic devices. *Nature* 420(6917):800-803.

Dalpian GM and Chelikowsky JR. 2006. Self-Purification in Semiconductor Nanocrystals. *Phys. Rev. Lett.* 96(22):226802.

Daugherty JE, Porteous RK, and Graves DB. 1993. Electrostatic forces on small particles in low-pressure discharges. *J. Appl. Phys.* 73(4):1617-1620.

Du H, Chen C, Krishnan R, Krauss TD, Harbold JM, Wise FW, Thomas MG, and Silcox J. 2002. Optical Properties of Colloidal PbSe Nanocrystals. *Nano Letters* 2(11):1321-1324.

Efros AL and Shklovskii BI. 1984. *Electronic Properties of Doped Semiconductors*. Berlin: Springer.

Erwin SC, Zu L, Haftel MI, Efros AL, Kennedy TA, and Norris DJ. 2005. Doping semiconductor nanocrystals. *Nature* 436(7047):91-94.

Fowler RH and Nordheim L. 1928. Electron Emission in Intense Electric Fields. *Proc. R. Soc. Lond. A* 119:173-181.

Fujii M, Mimura A, Hayashi S, and Yamamoto K. 1999. Photoluminescence from Si nanocrystals dispersed in phosphosilicate glass thin films: Improvement of photoluminescence efficiency. *Appl. Phys. Lett.* 75(2):184-186.

Goree J. 1994. Charging of particles in a plasma. *Plasma Sources Science and Technology* 3(3):400-406.

Gorla CR, Liang S, Tompa GS, Mayo WE, and Lu Y. 1997. Silicon and germanium nanoparticle formation in an inductively coupled plasma reactor. In *The 43rd national symposium of the American Vacuum Society*, 15: 860-864. Philadelphia, Pennsylvania (USA): AVS.

Gresback R, Holman Z, and Kortshagen U. 2007. Nonthermal plasma synthesis of size-controlled, monodisperse, freestanding germanium nanocrystals. *Appl. Phys. Lett.* 91(9):093119-3.

Guzelian AA, Katari JEB, Kadavanich AV, Banin U, Hamad K, Juban E, Alivisatos AP, Wolters RH, Arnold CC, and Heath JR. 1996. Synthesis of Size-Selected, Surface-Passivated InP Nanocrystals. *The Journal of Physical Chemistry* 100(17):7212-7219.

Han M, Gao X, Su JZ, and Nie S. 2001. Quantum-dot-tagged microbeads for multiplexed optical coding of biomolecules. *Nat Biotech* 19(7):631-635.

Hanif KM, Meulenberg RW, and Strouse GF. 2002. Magnetic Ordering in Doped Cd1-xCoxSe Diluted Magnetic Quantum Dots. *Journal of the American Chemical Society* 124(38):11495-11502.

Holm J and Roberts JT. 2009. Sintering, Coalescence, and Compositional Changes of Hydrogen-Terminated Silicon Nanoparticles as a Function of Temperature. *The Journal of Physical Chemistry C* 113(36):15955-15963.

Ifuku T, Otobe M, and Oda AIAS. 1997. Fabrication of Nanocrystalline Silicon with Small Spread of Particle Size by Pulsed Gas Plasma. *Jpn. J. Appl. Phys.* 36:4031-4034.

Knipping J, Wiggers H, Rellinghaus B, Roth P, Konjhodzic D, and Meier C. 2004. Synthesis of High Purity Silicon Nanoparticles in a Low Pressure Microwave Reactor. *Journal of Nanoscience and Nanotechnology* 4:1039-1044.

Kanzawa Y, Fujii M, Hayashi S, and Yamamoto K. 1996. Doping of B atoms into Si nanocrystals prepared by rf cosputtering. *Solid State Communications* 100(4):227-230.

Kruis FE, Fissan H, and Peled A. 1998. Synthesis of nanoparticles in the gas phase for electronic, optical and magnetic applications--a review. *Journal of Aerosol Science* 29(5-6):511-535.

Lampert MA, Many A, and Mark P. 1964. Space-Charge-Limited Currents Injected from a Point Contact. *Phys. Rev.* 135(5A):A1444.

Langof L, Fradkin L, Ehrenfreund E, Lifshitz E, Micic O, and Nozik A. 2004. Colloidal InP/ZnS core-shell nanocrystals studied by linearly and circularly polarized photoluminescence. *Chemical Physics* 297(1-3):93-98.

Lechner R, Stegner AR, Pereira RN, Dietmueller R, Brandt MS, Ebbers A, Trocha M, Wiggers H, and Stutzmann M. 2008. Electronic properties of doped silicon nanocrystal films. *J. Appl. Phys.* 104(5):053701-7.

Lewis KE, Golden DM, and Smith GP. 1984. Organometallic bond dissociation energies: laser pyrolysis of iron pentacarbonyl, chromium hexacarbonyl, molybdenum hexacarbonyl, and tungsten hexacarbonyl. *Journal of the American Chemical Society* 106(14):3905-3912.

Li L and Reiss P. 2008. One-pot Synthesis of Highly Luminescent InP/ZnS Nanocrystals without Precursor Injection. *Journal of the American Chemical Society* 130(35):11588-11589.

Littau KA, Szajowski PJ, Muller AJ, Kortan AR, and Brus LE. 1993. A luminescent silicon nanocrystal colloid via a high-temperature aerosol reaction. *The Journal of Physical Chemistry* 97(6):1224-1230.

Liu C, Holman ZC, and Kortshagen UR. 2009. Hybrid Solar Cells from P3HT and Silicon Nanocrystals. *Nano Letters* 9(1):449-452.

Mangolini L, Thimsen E, and Kortshagen U. 2005. High-Yield Plasma Synthesis of Luminescent Silicon Nanocrystals. *Nano Letters* 5(4):655-659.

Micic OI, Sprague JR, Curtis CJ, Jones KM, Machol JL, Nozik AJ, Giessen H, Fluegel B, Mohs G, and Peyghambarian N. 1995. Synthesis and Characterization of InP, GaP, and GaInP2 Quantum Dots. *The Journal of Physical Chemistry* 99(19):7754-7759.

Micic OI, Curtis CJ, Jones KM, Sprague JR, and Nozik AJ. 1994. Synthesis and Characterization of InP Quantum Dots. *The Journal of Physical Chemistry* 98(19):4966-4969.

Micic OI, Sprague J, Lu Z, and Nozik AJ. 1996. Highly efficient band-edge emission from InP quantum dots. *Appl. Phys. Lett.* 68(22):3150-3152.

Mott N. 1968. Metal-Insulator Transition. *Rev. Mod. Phys.* 40(4):677-683.

Murray CB, Norris DJ, and Bawendi MG. 1993. Synthesis and characterization of nearly monodisperse CdE (E = sulfur, selenium, tellurium) semiconductor nanocrystallites. *Journal of the American Chemical Society* 115(19):8706-8715.

Norris DJ, Yao N, Charnock FT, and Kennedy TA. 2001. High-Quality Manganese-Doped ZnSe Nanocrystals. *Nano Letters* 1(1):3-7.

Nozik AJ. 2002. Quantum dot solar cells. *Physica E: Low-dimensional Systems and Nanostructures* 14(1-2):115-120.

Otobe M, Kanai T, Ifuku T, Yajima H, and Oda S. 1996. Nanocrystalline silicon formation in a SiH4 plasma cell. *Journal of Non-Crystalline Solids* 198-200(Part 2):875-878.

Pi XD, Gresback R, Liptak RW, Campbell SA, and Kortshagen U. 2008. Doping efficiency, dopant location, and oxidation of Si nanocrystals. *Appl. Phys. Lett.* 92(12):123102-3.

Pi XD and Kortshagen U. 2009. Nonthermal plasma synthesized freestanding silicon–germanium alloy nanocrystals. *Nanotechnology* 20(29):295602.

Pratsinis SE. 1998. Flame aerosol synthesis of ceramic powders. *Progress in Energy and Combustion Science* 24(3):197-219.

Rafiq MA, Tsuchiya Y, Mizuta H, Oda S, Uno S, Durrani ZAK, and Milne WI. 2005. Charge injection and trapping in silicon nanocrystals. *Appl. Phys. Lett.* 87(18):182101-3.

Rafiq MA, Tsuchiya Y, Mizuta H, Oda S, Uno S, Durrani ZAK, and Milne WI. 2006. Hopping conduction in size-controlled Si nanocrystals. *J. Appl. Phys.* 100(1):014303-4.

Seeger K. 2004. *Semiconductor physics*. Springer.

Selmarten D, Jones M, Rumbles G, Yu P, Nedeljkovic J, and Shaheen S. 2005. Quenching of Semiconductor Quantum Dot Photoluminescence by a π-Conjugated Polymer. *The Journal of Physical Chemistry B* 109(33):15927-15932.

Selwyn GS, Singh J, and Bennett RS. 1989. In situ laser diagnostic studies of plasma-generated particulate contamination. *J. Vac. Sci. Technol. A* 7(4):2758-2765.

Shenai-Khatkhate DV, DiCarlo Jr. RL, and Ware RA. 2008. Accurate vapor pressure equation for trimethylindium in OMVPE. *Journal of Crystal Growth* 310(7-9):2395-2398.

Simánek E. 1981. The temperature dependence of the electrical resistivity of granular metals. *Solid State Communications* 40(11):1021-1023.

Spear W and Le Comber P. 1993. Substitutional doping of amorphous silicon. *Solid State Communications* 88(11-12):1015-1018.

Stegner AR, Pereira RN, Klein K, Lechner R, Dietmueller R, Brandt MS, Stutzmann M, and Wiggers H. 2008. Electronic Transport in Phosphorus-Doped Silicon Nanocrystal Networks. *Phys. Rev. Lett.* 100(2):026803.

Stegner AR, Pereira RN, Lechner R, Klein K, Wiggers H, Stutzmann M, and Brandt MS. 2009. Doping efficiency in freestanding silicon nanocrystals from the gas phase: Phosphorus incorporation and defect-induced compensation. *Phys. Rev. B* 80(16):165326.

Stoldt CR, Haag MA, and Larsen BA. 2008. Preparation of freestanding germanium nanocrystals by ultrasonic aerosol pyrolysis. *Applied Physics Letters* 93(4):043125.

Talapin DV, Gaponik N, Borchert H, Rogach AL, Haase M, and Weller H. 2002. Etching of Colloidal InP Nanocrystals with Fluorides: Photochemical Nature of the Process Resulting in High Photoluminescence Efficiency. *The Journal of Physical Chemistry B* 106(49):12659-12663.

Talapin DV and Murray CB. 2005. PbSe Nanocrystal Solids for n- and p-Channel Thin Film Field-Effect Transistors. *Science* 310(5745):86-89.

Wehrenberg BL, Yu D, Ma J, and Guyot-Sionnest P. 2005. Conduction in Charged PbSe Nanocrystal Films. *The Journal of Physical Chemistry B* 109(43):20192-20199.

Xie R, Battaglia D, and Peng X. 2007. Colloidal InP Nanocrystals as Efficient Emitters Covering Blue to Near-Infrared. *Journal of the American Chemical Society* 129(50):15432-15433.

Xu S, Kumar S, and Nann T. 2006. Rapid Synthesis of High-Quality InP Nanocrystals. *Journal of the American Chemical Society* 128(4):1054-1055.

Appendix A

A.1 Hybrid Solar Cells from P3HT and InP Nanocrystals.

The following results were obtained with Chin-Yi Liu.

InP nanocrystals were synthesized with the process described in Chapter 2. After synthesis, the NCs were transported air-free to the glovebox. DCB was added to a vial containing a known mass of NCs on a stainless steel mesh. The solution was sonicated and the mesh was removed resulting in a suspension of InP NCs in DCB. A solution of poly-3(hexylthiophene) (P3HT) in DCB was added to the suspension and the weight fraction investigated was 20-50% InP to P3HT.

The method used to fabricate the devices was similar to the one described by Lui et al.[1] The device structure is shown in Figure A.1. The suspension was spun at 700 rpm for 1 min onto a glass substrate prepared with a patterned ITO and an electron blocking layer of PEDOT:PSS. Aluminum contacts were then evaporated on top of the blended structure of P3HT/InP NCs.

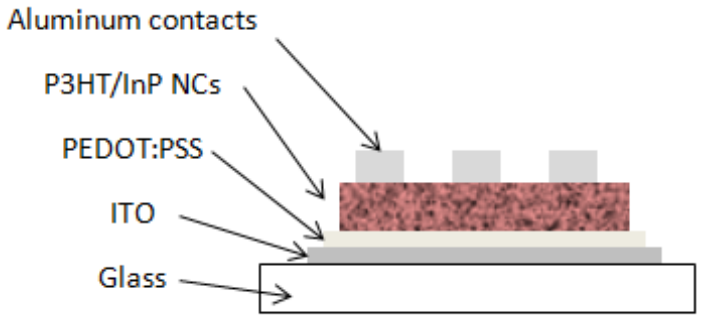

Figure A.1: Device structure of hybrid solar cell with P3HT and InP NCs.

This device design allows for a variety experimental investigations: the ratio between P3HT and InP NCs was adjusted to optimize exciton dissociation at the P3HT/InP interfaces, the concentration of the blended solution affected the thickness of the film, changing the NC size would to tune the NC bandgap, the plasma chemistry was adjusted to influence the NC stoichiometry, and sample annealing was used to remove defects in NCs and crystallize the P3HT.

The I-V characteristics for a device fabricated with InP NCs having a mean diameter of 4 nm with 50 % InP/P3HT by weight are shown in Figure A.2. The open circuit voltage (V_{oc}) was 0.4 V with a short circuit current (J_{sc}) of 10^{-3} mA/cm^2. After the device was annealed at 150 °C for 1 hour, the V_{oc} increased to 0.45 V and the J_{sc} increased to ~0.05 mA/cm^2. It is believed that the InP NCs surface restructuring along with the P3HT crystallization were induced by the annealing step resulting in increase device performance. However these results were significantly lower than for devices fabricated by Chin-Yi Liu with Si NCs and P3HT.[1]

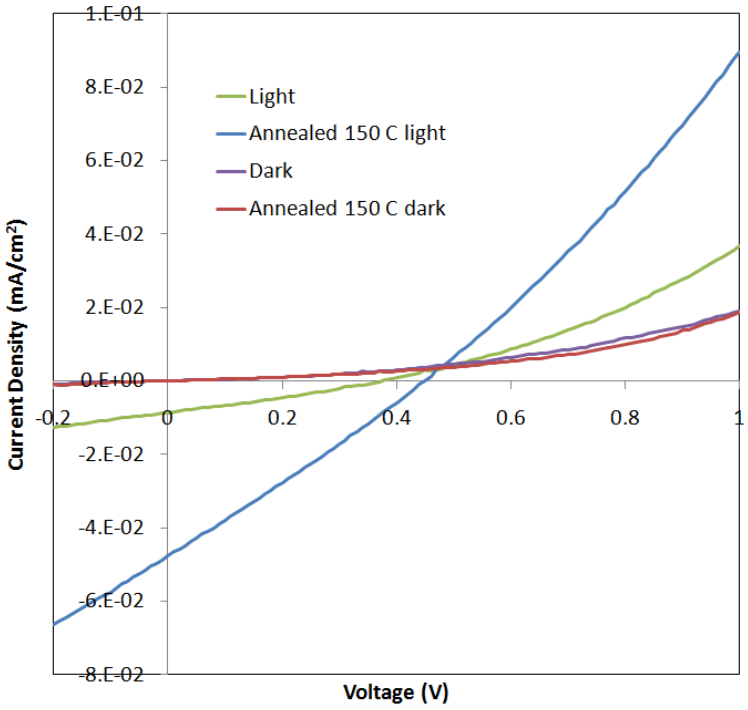

Figure A.2: Effect of 150 °C annealing for hybrid solar cell of P3HT and InP NCs with mean size of 4 nm.

Since annealing had such a positive effect on device performance, an additional step was included, to preheat the NCs to remove any physically absorbed atoms and allow for restructuring of the surface prior to device fabrication. This was done in a glove box in a close-container with a solution of DCB and InP NCs was heated to 230 °C for 1 hour. The device was then fabricated as described above. A comparison of the performances of unheated, preheated, and preheated with post annealing films are shown in Figure A.3. Films that have not been pre-heated or annealed showed a small V_{oc} and J_{sc}. Both treatments of NC pre-heating and film annealing improved the device performance, yet such improvement was not substantial.

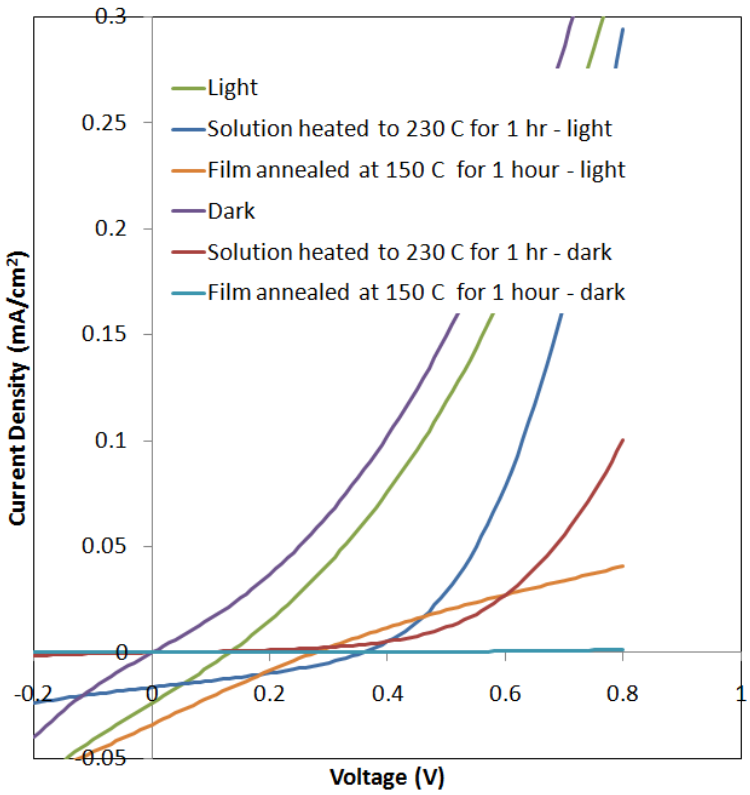

Figure A.3: I-V characteristics of P3HT/InP NC solar cells for different thermal treatments for: InP NCs in DCB heated for 1 hour at 150 °C, film annealed after solution heating, and no thermal treatment.

No significant improvement was found for changing the weight concentration of InP NCs to P3HT. Since the energetics of the device may not be favorable for 4 nm NCs, smaller NCs with a wider bandgap were chosen to determine if device properties could be improved.

The I-V characteristics for a device fabricated with InP NCs with a mean diameter of ~2.4 nm can be found in Figure A.4. Higher currents were observed for this device, however the photovoltaic response was still poor.

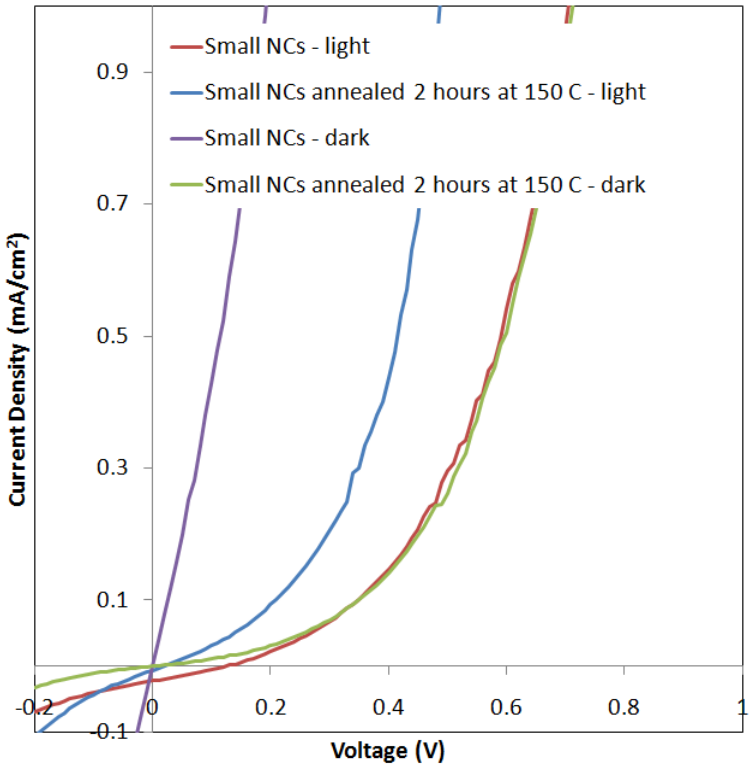

Figure A.4: I-V characteristics of P3HT/InP devices with NCs having mean size ~ 2.4 nm

We attribute the poor photovoltaic responses for all devices to two potential problems: the first cause could be contact of the InP layer between the NCs and the hole blocking layer, leading to current being able to go from the ITO layer to the aluminum, a scenario compatible with the poor diode behavior observed; second the presence of defects or traps in the InP NCs could lead to photogenerated carriers to be unable to dissociate and lead to photocurrent.

Future work should focus on using InP NCs which have been capped with a shell of ZnS to remove trap sites and defects. This treatment allows for a better dissociation of

excitons at the interface between the polymer and the NCs. It is also promising for a better transport of carriers through the network.

Another major issue with these devices has to do with the continuity of networks of NCs going through the whole device. This can be studied and improved by using a different solvent in the fabrication of the device. Other geometries like a bilayer structure may also improve device performance and allow for understanding of the effects of the InP NCs.

1. Liu, C.; Holman, Z.C.; Kortshagen, U.R. Hybrid Solar Cells from P3HT and Silicon Nanocrystals. *Nano Lett.* ***2009***, 9, 449-452.

Appendix B

B.1 Synthesis of Ge NCs

A variety of precursors have been used to synthesize germanium nanocrystals using a nonthermal plasma reactor as described previously. Germanium tetrachloride ($GeCl_4$), germane (GeH_4) and tetraethylgermane (TEG) have all been tested. Germanium tetrachloride was first used to synthesize Ge NCs. Control over size, shape, and crystallinity could be achieved through residence time, power, and plasma chemistry.[1] Yet, contrary to reports in literature of high efficiency PL, none was observed, due to the possible presence of highly electronegative chlorine at the surface leading to non-radiative recombination of excitons.

Tetraethyl germane was an obvious choice for a safe precursor, since germane is highly toxic. Both of these precursors were tested to determine if synthesis of NCs was possible. Figure B.1 shows a TEM micrograph of Ge NCs synthesized with TEG and lattice fringes of the (111) planes of germanium are clearly present. Similarly Figure B.2 shows a TEM image of Ge NCs synthesized from GeH_4. Raman (Figure B.3) and XRD (Figure B.4) spectra show highly crystalline material, but no PL in the visible or infrared was observed.

EPR measurements were performed with Andre Stegner and Prof. Martin Stutzmann done on boron doped Ge NCs with diameters of 10 nm and Figure B.5 shows the mass normalized signals. We see that there is no change in the signal as a function of the doping concentration from 0 to 4% dopants per germanium atoms. The lack of change in EPR signal is probably due to boron's electron acceptor properties, making it difficult to see changes in dangling bond densities. Using an electron donor such as phosphorus should allow for noticeable changes in the EPR spectra.

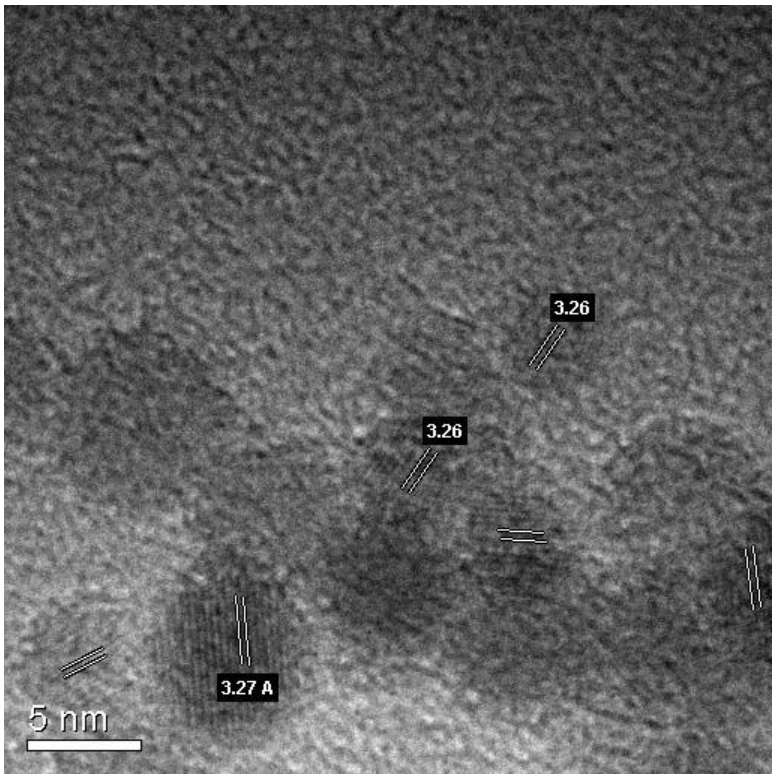

Figure B.1: TEM image of Ge NCs synthesized with tetraethyl germane.

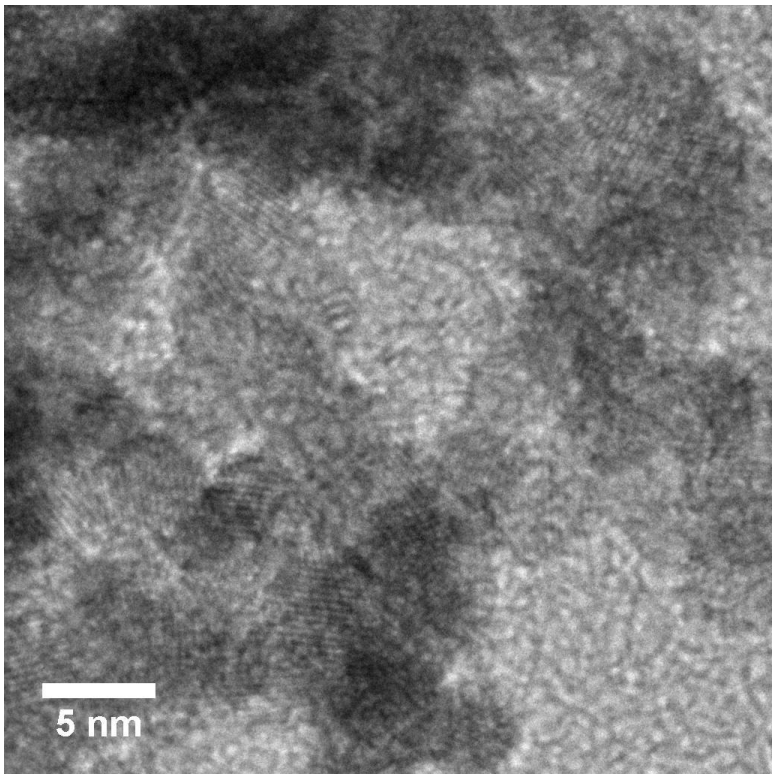

Figure B.2: TEM image of Ge NCs synthesized with germane.

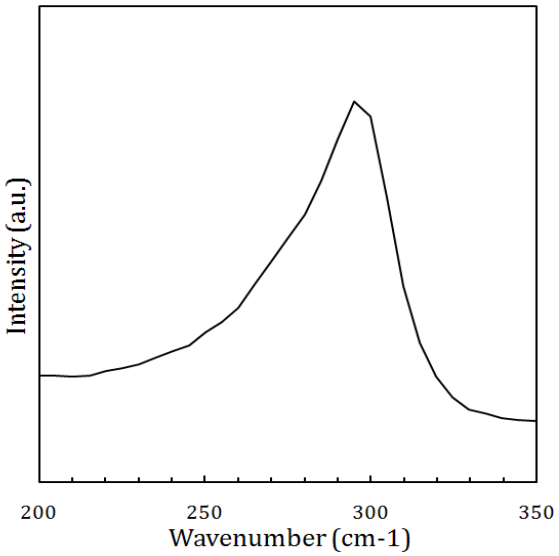

Figure B.3: Raman spectra of Ge NCs from germane. Average size ~ 4 nm determined by TEM.

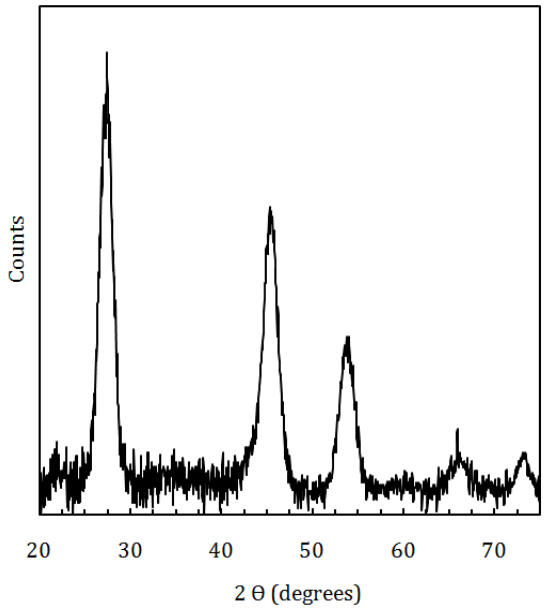

Figure B.4: XRD spectra of Ge NCs synthesized with germane.

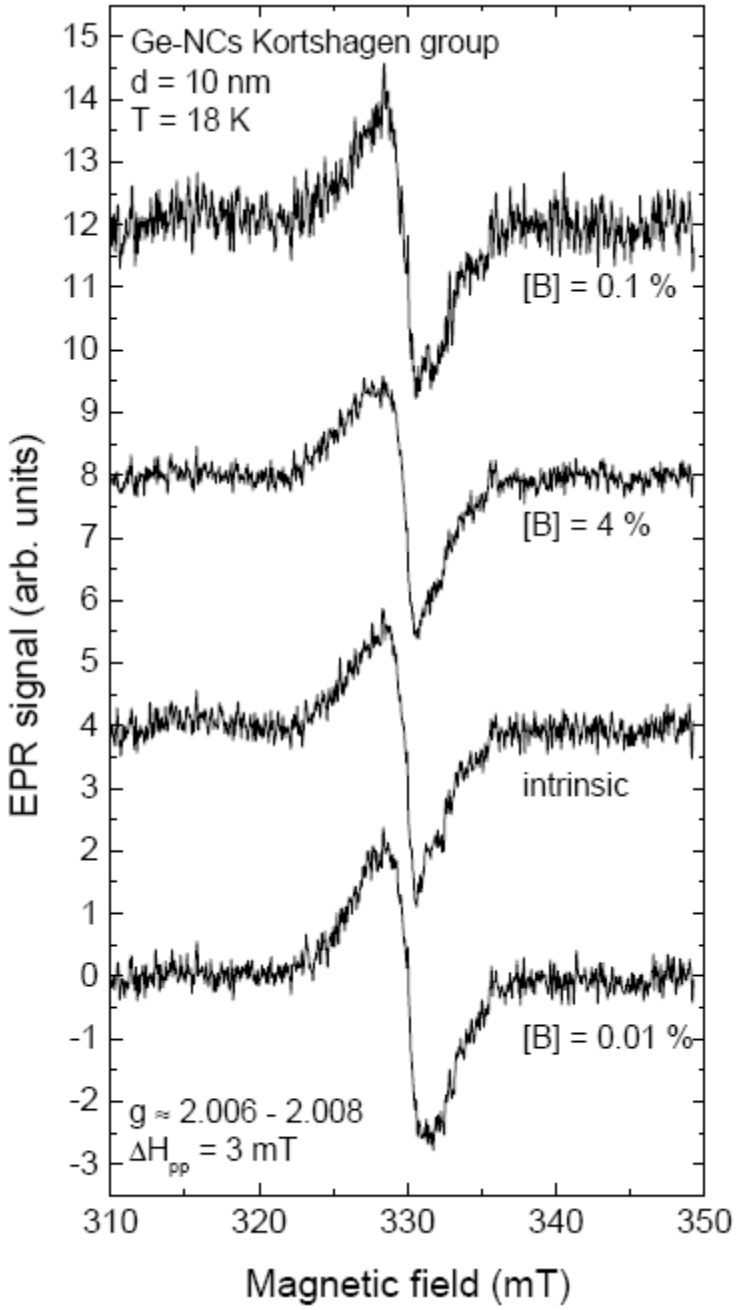

Figure B.5: Mass normalized EPR signal from boron doped Ge NCs. This work was done with Andre Stegner and Martin Stutzmann. No noticeable differences in defect level for different dopant concentrations.

1. Gresback, R.; Holman, Z.; Kortshagen, U. Nonthermal plasma synthesis of size-controlled, monodisperse, freestanding germanium nanocrystals. *Appl. Phys. Lett.* **2007** 91, 093119-3.